Semiannual Progress Report

(01 June 1993 - 30 November 1993)

ONR CONTRACT INFORMATION

Contract Title: Stress-Corrosion Resistant Ultrahigh-Strength Steels

Performing Organization: Northwestern University Materials Research Center

Principal Investigator Prof. G. B. Olson
Co-Investigators: Prof. D. E. Ellis
Prof. A. J. Freeman

Contract Number: N00014-90-J-1363

R & T Project Number: met0012---07

ONR Scientific Officer: Dr. George Yoder

"Original contains color plates: All DTIC reproductions will be in black and white"

SUMMARY

Based on the Rice-Wang thermodynamic model of intergranular embrittlement, total energy calculations employing the FLAPW, DMol and DVM techniques address the electronic basis of the segregation energy difference between grain boundaries (GB) and free surfaces (FS) controlling the embrittlement potency of a segregating solute. Precise FLAPW calculations employing large supercells with structural relaxations determined by DMol predict the embrittling effect of P in Fe, and indicate that B is neutral or weakly cohesion enhancing in Fe. The embrittlers P and S are found to behave as "embedded" atoms with negligible hybridization with Fe, while B hybridizes to form directional σ bonds which significantly raise its relative energy on the free surface. Magnetic contributions are found to decrease both the embrittling potency of P and the cohesion enhancing ability of B. Toward greater precision of segregation energy calculations, DMol calculations have been initiated with modified boundary conditions to allow for GB free volume. DVM cluster calculations are applied to explore the third-element interaction with substitutional Mo at the GB core. A cohesion enhancing effect of Mo more than compensates the embrittling effect of P. GB fracture strength is measured in UHS steels and correlated with segregation of P and S.

1. INTRODUCTION

The objectives of this research are to establish the electronic-level mechanisms of intergranular embrittlement in Fe-base alloys, and to design and produce improved grain boundary compositions for enhanced stress-corrosion resistance in ultrahigh-strength steels. Based on the Rice-Wang thermodynamic model of impurity-induced embrittlement, our electronic calculations focus on the origins of the energy difference of solutes in the Fe grain boundary (GB) and free surface (FS) environments as the key quantity governing embrittlement potency.

Our paper published last year (Wu, Freeman and Olson [1]) reported the application of the precise Full-Potential Linear Augmented Plane-Wave (FLAPW) Method to comparison of the energy and electronic structure of P in the Fe $\Sigma 3$ $[1\bar{1}0]$ (111) GB and corresponding Fe (111) FS environments. It was shown that if Fe structural relaxations are neglected, the chemical bonding of P is actually greater in the GB than the FS, in opposition to its embrittling effect. Our recently published paper comparing P and B on the Fe (111) FS (Wu, Freeman, and Olson [2]) showed that the degree of structural relaxation in the FS environment is relatively small. Also recently published is our study of the detailed structural relaxations of the Fe $\Sigma 3$ $[1\bar{1}0]$ (111) GB with and without P, employing the DMol cluster method (Tang, Freeman, and Olson [3]). This study showed that the cluster size had to be increased from 53 to 91 atoms to fully treat the relatively long-range relaxations associated with the GB. The clean GB was found to relax locally to an ω-phase structure, and a substantial energy penalty is associated with reconstruction of the GB by P to an "anti-ω" structure.

The detailed reconstruction of the GB has been taken into account in precise FLAPW calculations comparing P in the GB and FS environments employing larger 24 layer supercells for the GB and 13 layer supercells for the FS in order to achieve the most precise energy comparisons currently possible. A paper detailing these definitive calculations demonstrating the embrittling behavior of P (Wu, Freeman and Olson [4]) was provided with our previous progress report. A new paper detailing the comparison of precise FLAPW calculations for P and B in the GB and FS environments (Wu, Freeman and Olson [5]) is attached as Appendix A. A revised manuscript describing further DMol studies of the structural relaxations and bonding behavior of B and S in the same GB (Tang, Freeman and Olson [6]) is attached as Appendix B.

A major goal of our research is the exploitation of third-element interactions to enhance GB cohesion and minimize embrittlement susceptibility. While the highly precise FLAPW and

DMol calculations require use of CRAY supercomputing facilities provided by NSF, a survey of third-element interaction effects is being conducted employing the cluster Discrete Variational Method (DVM) which can be run on the HP730 Workstation obtained last year under the subject ONR grant. A brief description of its application to P embrittlement is included in a recent review paper (Ellis [7]) and a full account is given in a manuscript (Sagert, Ellis and Olson [8]) provided with the previous report which explores the effect of Mo on the P embrittlement of the same Fe $\Sigma 3$ $[1\bar{1}0]$ (111) GB.

Our recent results on the gettering of impurities by novel compounds in rapidly solidified steels were summarized in a conference abstract paper (Ghosh and Olson [9]) also provided with the previous report.

2. EMBRITTLEMENT ENERGETICS

Table 1 of Appendix A gives a comprehensive summary of our most precise FLAPW calculations of the energy contributions to the effects of both P and B on the cohesion of the Fe $\Sigma 3$ $[1\bar{1}0]$ (111) GB. The values for Fe-P are from the large supercell calculations of Ref. [4] employing the GB relaxations of Ref. [3], while the values for Fe-B are from very recently completed calculations employing the same large supercells with the GB relaxations of App. B [6]. Values are listed for the binding energies per impurity atom (relative to an isolated impurity monolayer) for the GB (ΔE_b) and FS (ΔE_s) for (a) unrelaxed configurations defining the "chemical" interaction, (b) the energy difference associated with boundary relaxation defining the "mechanical" energy penalty of boundary reconstruction, and (c) the total energy change for relaxed configurations taking into account both contributions. Also listed are the values for non-spin-polarized or nonmagnetic (NM) calculations to compare with the spin-polarized or ferromagnetic (FM) calculations. These ultimately define the magnetic contribution to the ΔE_b-ΔE_s energy differences governing embrittlement potency.

The Fe-P results for the unrelaxed case are similar to the earlier small cell results [1] in that the pure chemical contribution to ΔE_b-ΔE_s is cohesion enhancing by -0.75eV. This is more than offset, however, by the mechanical reconstruction energy penalty which is much larger in the GB, making the final ΔE_b-ΔE_s positive and therefore embrittling by +1.60eV in the nonmagnetic case and +0.79eV in the ferromagnetic case. The results for Fe-B show that compared to P the B has a similar binding energy in the GB (with or without relaxation) but a significantly smaller binding energy on the FS consistent with the earlier calculations of Ref. [2].

Experimental estimates of ΔE_b-ΔE_s are +0.5eV for P and -0.8eV for B (with an uncertainty of ~0.1eV), consistent with observed behavior of P as an embrittler and B as a cohesion enhancer. The calculated difference between P and B is reasonably in line with experiment but the individual ΔE_b-ΔE_s values are shifted towards embrittlement by 0.3 to 0.8eV. This may be due to a systematic error in the calculated relaxation energies which are the most difficult quantity to determine.

Toward improved calculation of GB relaxations with and without P and B, revised DMol cluster calculations have now been initiated with modified boundary conditions. The cluster models are relaxed at constant volume, locking cluster surface atoms in place to minimize free surface effects arising from the finite cluster size. While the previous calculations employed a volume based on the initial CSL GB configuration, the new calculations employ an initial volume taken from the embedded-atom method (EAM) calculations of Krasko [10] for the same boundaries. This allows for GB free volume that was not allowed in the earlier calculations, and may have provided an effective pressure which raised the relative GB energy in the presence of the segregants. The new calculations actually give a higher cluster energy with the free volume allowed, but we believe this is an artifact of the finite cluster size. FLAPW calculations with the new relaxed configurations will determine if the GB energy is now lower in the bulk environment. We are hopeful that this modification will resolve the apparent systematic error in GB relaxation energies.

While calibration of our calculations against experimental energies is important to assess whether our methods realistically incorporate the essential physics of the problem, most important is an understanding of the trends between species from which insights can be gleaned for grain boundary design. Fortunately, the chemical bonding trends we observe are much less sensitive to cell size and details of structural relaxation.

3. CHEMICAL BONDING

To assess the chemical bonding behaviors, Figure 1 shows computed charge transfer plots comparing P and B in the GB and FS environments. These are obtained by subtracting the superimposed charge densities of the pure components from the computed total charge density. Contours start from 1×10^{-3} e/a.u.^{3} and increase successively by a factor of $2^{1/4}$; green, yellow, red and pink colors denote positive differences, and light and dark blue denote negative differences. While the results for P are similar to those obtained in our earlier small cell calculations [1] the plots in Figure 1 are taken from the large supercell calculations of Appendix A [5].

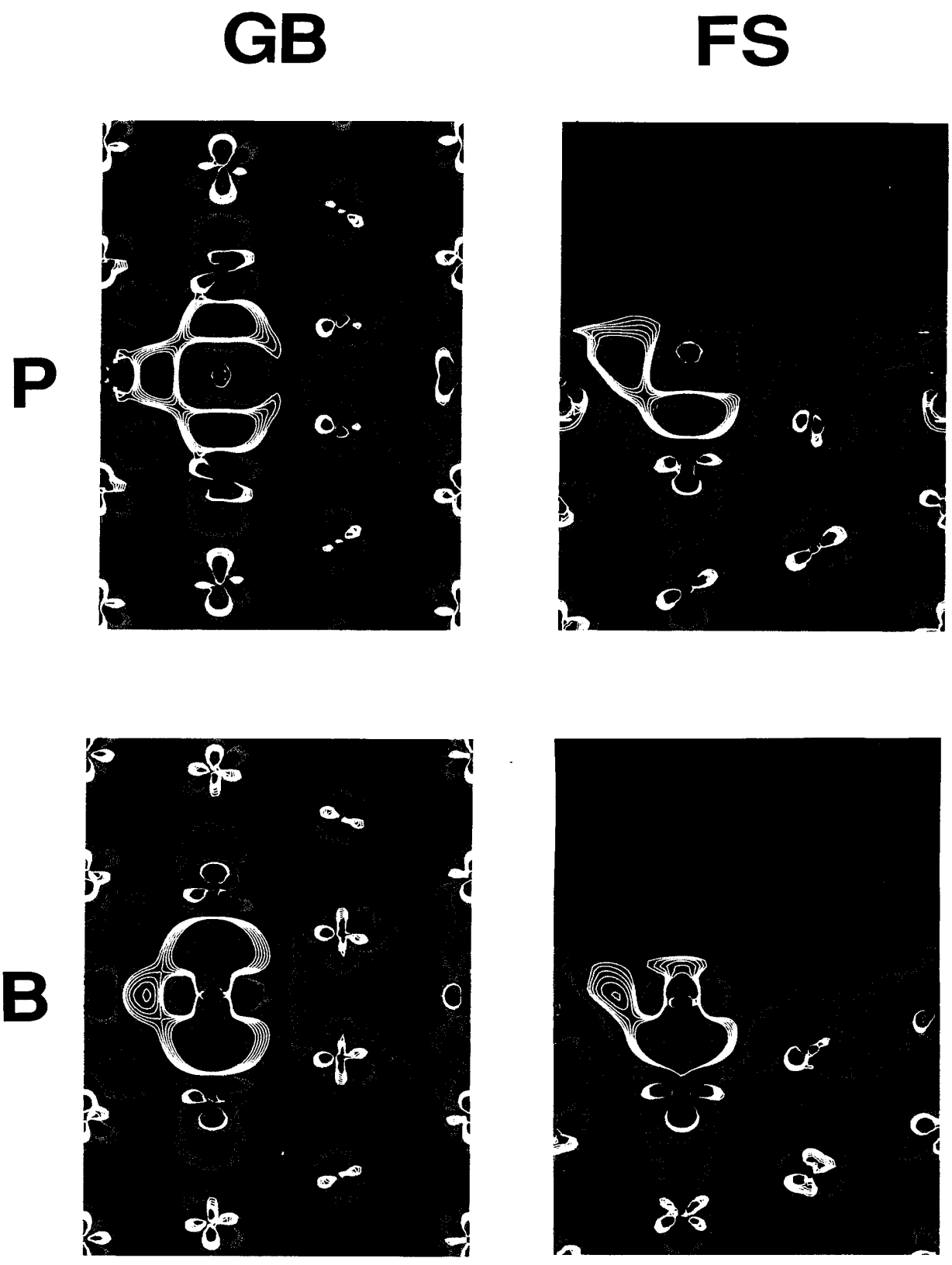

Figure 1. Calculated valence charge density difference for P and B in grain boundary (GB) and free surface (FS) environments. Contours start from 1×10^{-3} e/a.u.^{3} and increase successively by a factor of $2^{1/4}$; green, yellow, red and pink colors denote positive differences, light and dark blue denote negative differences.

A deeper interpretation of the charge transfer plots has emerged from detailed analysis of specific molecular orbital wave functions in the DMol cluster calculations for P in Ref. [3] and for B and S in App. B [6]. As illustrated for an S 3p orbital ($1\acute{a}_2$) in Fig. 3a of App. B and for a B 2p orbital ($4\acute{a}_2$) in Fig. 6 of App. B, we find that the 3p electrons of the embrittlers P and S actually show very little hybridization with Fe, while the 2p electrons of B do hybridize with Fe to give significant covalent σ bonding normal to the GB plane. Although the local charge transfer maxima for P in Figure 1 resemble covalent bonds, we interpret the behavior of P as an "embedded" atom which simply interacts electrostatically with the potential of the surrounding Fe atoms, the local charge transfer maxima corresponding predominantly to P3p electrons which are not significantly hybridized with the neighboring Fe. This electrostatic interaction is relatively unchanged in character on going from the GB to the FS (although the P 3p energy levels move in response to the changed potential, and this slightly favors interaction in the GB environment). In contrast, the local charge transfer maxima for B do reflect directional covalent σ bonding, an important consequence of which is the "dangling bond" above the B atom on the FS as revealed in Figure 1. We thus associate this directional bonding character of B with the larger chemical contribution to ΔE_b-ΔE_s, the primary contribution to its differing behavior relative to P.

The corresponding spin density difference plots for the configurations of Figure 1 are shown in Figure 2, employing the same units and color code. Similar to the earlier small cell calculations of Ref. [1] it is evident that the impurities reduce the magnetic moment (blue) of near neighbor Fe atoms in both the GB and FS environments. An important feature revealed by the new large cell calculations is that Fe atoms further from the impurities have enhanced moments (red), and the magnetic effects have a significantly longer range than the net charge transfer effects. The change of magnetic moments of the atoms of figure 2 are summarized in Table 2 of Appendix A [5]. Also listed are the moments in the relaxed clean Fe boundary where the ω phase transition causes an antiferromagnetic state [3]. The net effect of the longer range magnetic interactions and the ω relaxation of the clean boundary is summarized by the magnetic energy increments in the last column of Table 1 of Appendix A [5]. In contrast to the earlier small cell estimates [1], the contributions of magnetism actually decrease the embrittlement potency of P by -0.81eV. The magnetic effect for B is the opposite, decreasing its cohesion enhancing effect by +0.38eV.

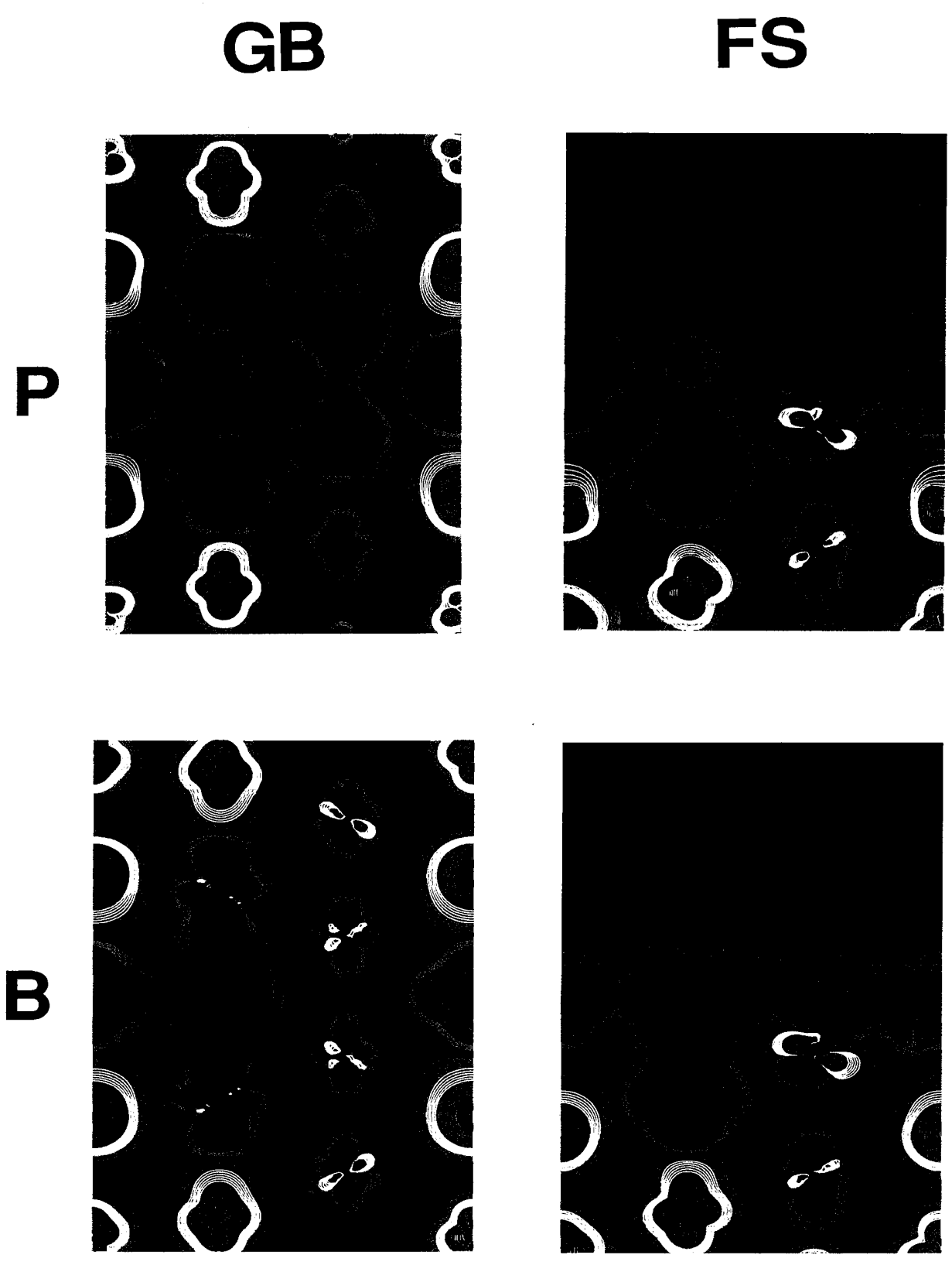

Figure 2. Calculated spin density difference for P and B in grain boundary (GB) and free surface (FS) environments. Units and color code as in Figure 1.

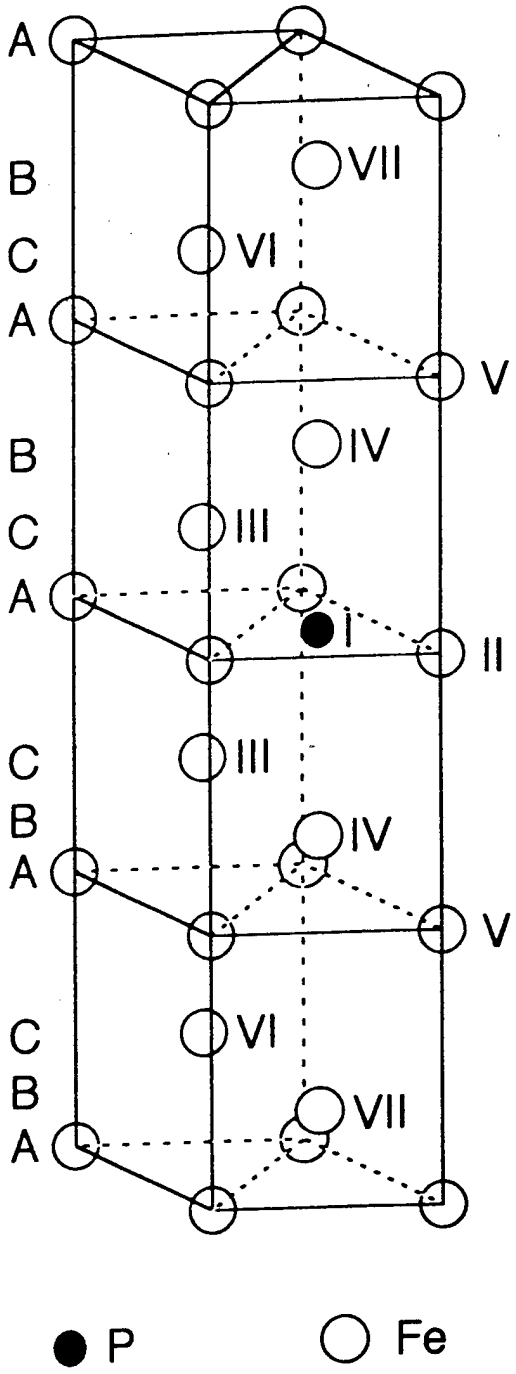

Figure 3. Labelling of atomic positions employed in grain boundary and free surface cluster models.

Table 1

Integrated Charge and Energy Densities Between Atoms

(Values taken for bond radii = 0.53 Å,

Excluded length = 0.26 Å)

Clean Mo/Fe Grain Boundary Cluster (34 Atoms)

Bond	Bond Length (Å)	Total Charge (e)	Total Energy (eV)
Vac(I)-Mo(II)	1.81	0.40	-1.31
Vac(I)-Fe(III)	2.17	0.89	-2.76
Vac(I)-Fe(IV)	1.82	0.83	-2.32
Mo(II)-Mo(II)	3.51	1.00	-2.75
Fe(III)-Fe(III)	2.17	1.34	-3.88

P/Mo/Fe Grain Boundary Cluster (35 Atoms)

Bond	Bond Length (Å)	Total Charge (e)	Total Energy (eV)
P(I)-Mo(II)	1.81	0.80	-1.41
P(I)-Fe(III)	2.17	1.19	-3.77
P(I)-Fe(IV)	1.82	1.09	-3.00
Mo(II)-Mo(II)	3.51	1.34	-3.45
Fe(III)-Fe(III)	2.17	1.33	-4.05

Clean Mo/Fe Free Surface Cluster (35 Atoms)

Bond	Bond Length (Å)	Total Charge (e)	Total Energy (eV)
Vac(I)-Mo(II)	1.86	0.53	-0.26
Vac(I)-Fe(III)	2.15	0.87	-1.73
Vac(I)-Fe(IV)	1.61	0.78	-1.37
Mo(II)-Mo(II)	3.52	1.29	-0.66

P/Mo/Fe Free Surface Cluster (36 Atoms)

Bond	Bond Length (Å)	Total Charge (e)	Total Energy (eV)
P(I)-Mo(II)	1.86	0.98	-0.36
P(I)-Fe(III)	2.15	1.20	-2.16
P(I)-Fe(IV)	1.61	1.10	-0.94
Mo(II)-Mo(II)	3.52	1.50	-1.59

4. ALLOYING EFFECTS

As described in the previous progress report, the DVM cluster method is being applied to the third-element interaction with Mo employing the same atomic configurations as in Fig. 1, but with a substitutional monolayer of Mo at the GB core. The Mo-P interaction in the intergranular embrittlement of Fe is fairly well studied experimentally, the evidence indicating that grain boundary cosegregation of Mo and P results in a reduction of embrittlement. Although the charge transfer behavior looks quite different from the binary Fe-P case of Figure 1, the P is found to still show "embedded" behavior with no significant hybridization with either Fe or Mo. There is however enhanced charge transfer from Mo to P in association with its greater electronegativity difference, resulting in a greater ionic bonding component and an electrostatic attraction of the P 3p electrons to the region adjacent to the Mo. The behavior is similar in the GB and FS environments, but with slightly greater charge transfer (and ionic interaction) on the FS. The energetic result is that Mo attracts P in both environments, but slightly more on the FS giving an increased chemical contribution to ΔE_b-ΔE_s for P of +0.8eV. However, this apparent increased embrittlement potency of P in the presence of Mo is found to be more than compensated by the direct cohesion enhancing effect of Mo. Hence the attraction of Mo to the GB by segregated P (with a Mo-P interaction energy of ~-1eV per atom) will overall enhance boundary cohesion.

The origin of the Mo cohesion enhancement is being investigated in terms of detailed local bonding. Labelling atomic positions according to the scheme of Figure 3 with Mo occupying site II, Table 1 summarizes integrated bond charges and energies. The bond volume is defined by a cylinder of 0.53Å radius with a length determined by excluding an 0.26Å distance from the atomic cores. Bond energy is seen to correlate well with bond charge with the notable exception of the Mo (II)-Mo(II) bonds which have an anomolously small bond energy. This is particularly noticeable for the clean Mo/Fe free surface cluster where the Mo(II)-Mo(II) bond has the highest bond charge (1.29e) but second smallest bond energy of -0.66eV. Much of the charge associated with these bonds apparently involves unfavorable energetic states relative to the Mo ground state, giving in-plane metal-metal bonds which are less energetically stable than the original Fe(II)-Fe(II) bonds. That this behavior is more pronounced on the FS than the GB may be very significant to GB cohesion. Unusual behavior of Mo in the GB environment was also reported by Dr. G. Krasko of ARL at our SRG subgroup meeting at Harvard in December, based on LMTO-ASA calculations. This behavior will be investigated further and compared with that of embrittling Mn to more clearly establish the electronic features of cohesion enhancing alloying elements for alloy design.

5. EXPERIMENTS

Results described in our previous progress report demonstrated that with careful avoidance of Si contamination, the rapid solidification of a model 0.4C Ni-Mo steel after late addition of La to a melt deoxidized with Zr+Ti successfully reproduced our earlier finding of La-P-O compounds which efficiently getter P. Rather than the highly stable La_2O_2S found earlier, however, the S was found to be gettered in the form of TiS. Analytical microscopy identified the P gettering phases as predominantly $LaPO_4$ and $La_7P_3O_{18}$. Further study of material deoxidized with Zr+Al revealed La_2O_2S as the dominant S gettering phase, and led to the discovery of ZrP as a P gettering phase as reported in Ref. [9]. Further correlation of gettering phases with melt deoxidation practice, aided by thermodynamic modeling, will address predictive control of impurity gettering.

As part of his surface analytical study of embrittling impurities under AASERT support, Graduate Student David Spaulding has measured the grain boundary fracture strength in polycrystalline tensile specimens of model UHS steels in which he previously measured the grain boundary segregation of P and S as a function of tempering time by Scanning Auger Microanalysis. The high yield strength of these alloys allowed fracture strength to be measured under well defined homogeneous elastic loading conditions. Correlation of boundary strength with the predicted reduction in ideal thermodynamic work of fracture will allow a more precise test of the Rice-Wang model than previous correlations with shifts in ductile-brittle transition temperature. Further experiments will quantify the effect of hydrogen charging.

6. REFERENCES (* denotes papers acknowledging ONR support.)

* 1. R. Wu, A. J. Freeman and G. B. Olson, "On the Electronic Basis of the Phosphorus Intergranular Embrittlement of Iron," J. Mater. Res. 7 (1992) 2403-2411.

* 2. R. Wu, A. J. Freeman and G. B. Olson, "Effects of P and B Adsorbates on the Fe (111) Surface," Phys. Rev. B 47 (1993) 6855-6858.

* 3. S. Tang, A. J. Freeman and G. B. Olson, "Phosphorus-Induced Relaxation in an Iron Grain Boundary: A Cluster Model Study," Phys. Rev. B 47 (1993) 2441-2445.

* 4. R. Wu, A. J. Freeman and G. B. Olson, "The Nature of Phosphorus Embrittlement of the Fe $\Sigma 3$ $[1\bar{1}0]$ (111) Grain Boundary," submitted to Phys. Rev. B.

* 5. R. Wu, A. J. Freeman and G. B. Olson, "First Principles Determination of the Effects of P and B on Fe Grain Boundary Cohesion," submitted to Phys. Rev. B.

* 6. S. Tang, A. J. Freeman and G. B. Olson, "Local Density Studies of the Structure and Electronic Properties of B and S in an Fe Grain Boundary," submitted to Phys. Rev. B.

* 7. D. E. Ellis, "Theory of Electronic Properties of Metal Clusters and Particles," in Metal Cluster Compounds, ed. L. J. de Jongh, (Kluwer, Dordrecht, 1993) in press.

* 8. L. P. Sagert, D. E. Ellis and G. B. Olson, "The Effect of Molybdenum on the Phosphorus Embrittlement of Iron," in preparation.

* 9. G. Ghosh and G. B. Olson, "Impurity Gettering in Rapidly Solidified Advanced Steels," in Proc. 51st Ann. Mtg. MSA, eds. G. W. Bailey and C. L. Reider (San Francisco Press, 1993) pp. 746-747.

10. G. L. Krasko, in Structure and Properties of Interfaces in Materials, eds. W. A. T. Clark, U. Dahmen and C. L. Briant, MRS Symp. Proc. 238 (MRS, Pittsburgh, 1991) p. 481.

APPENDICES

Appendix A "First Principles Determination of the Effects of P and B on Fe Grain Boundary Cohesion," R. Wu, A. J. Freeman and G. B. Olson, submitted to Phys. Rev. B.

Appendix B "Local Density Studies of the Structure and Electronic Properties of B and S in an Fe Grain Boundary," S. Tang, A. J. Freeman and G. B. Olson, to Phys. Rev. B.

APPENDIX A

Submitted to Phys. Rev. B

First Principles Determination of the Effects of P and B on Fe Grain Boundary Cohesion

Ruqian Wu[1], A.J. Freeman[1] and G.B. Olson[2]

[1] *Department of Physics & Astronomy, Northwestern University, Evanston, IL 60208*

[2] *Department of Materials Science and Engineering, Northwestern University, Evanston, IL 60208*

The effects of P and B impurities on the thermodynamic, electronic and magnetic properties of both the free Fe(111) surface and FeΣ3[1$\bar{1}$0] (111) grain boundary (GB) are investigated using the local density full potential linearized augmented plane wave method. We find that the spatial anisotropy of the impurity-Fe bonding plays a key role in the relative cohesion of the FeΣ3[1$\bar{1}$0] (111) GB. The segregation energies of P and B (relative to an isolated monolayer) are almost equal in the GB environment even when the impurity-induced structural relaxation in the FeΣ3[1$\bar{1}$0] (111) GB is considered. For P, the segregation energy at the free surface is lower than at the GB by -0.81 eV mainly due to the large relaxation energy in Fe GB. This energy difference is consistent with the observed embrittlement potency of P as described by the Rice-Wang thermodynamic model of Gb embrittlement. The bonding of P in both environments is electrostatic in nature, shows no significant hybridization with

---

December 30, 1993/w24.tex

Fe. In contrast, B shows strong hybridization with Fe giving directional bonding normal to the GB plane which increases the relative energy on the Fe(111) surface, in line with the relative cohesion enhancing effect of B. Magnetic contributions reduce both the embrittling effects of P and the cohesion enhancing effect of B.

61.70.Ng, 81.40.Np, 73.20.Hp, 75.30.Hx

I. INTRODUCTION

A thermodynamic theory developed by Rice and Wang [1, 2] describes the mechanism of metalloid-induced intergranular embrittlement through the competition between dislocation crack blunting and brittle boundary separation. While crystal plasticity considerations show interesting directional effects on the relative ease of dislocation emission from the crack tip, tested in critical bicrystal experiments, the most striking result of the analysis is the prediction that the potency of a segregating solute in reducing the "Griffith work" of brittle boundary separation is a linear function of the difference in segregation energy for that solute at a grain boundary (GB) ΔE_b, and a free surface (FS), ΔE_s. Simply put, a solute with a positive energy difference ΔE_b - ΔE_s (i.e., ΔE_b is less negative) will be a more potent embrittler, or vice versa. The validity of this hypothesis has been supported experimentally for Fe-base materials for which significant of data exist for both the relative embrittling potencies of solutes and the relevant surface thermodynamic quantities [3].

A predictive theory of intergranular cohesion can be developed by directly determining both ΔE_b and ΔE_s on an equal footing with present state-of-the-art energy band approaches; this offers the promise of major improvements in boundary cohesion sensitive properties such as the stress corrosion resistance of ultra-high strength steels. To this end, we have carried out full-potential linearized augmented plane wave (FLAPW) total energy calculations to investigate the effects of a phosphorus impurity in the FeΣ3[1$\bar{1}$0] (111) GB and on the corresponding Fe(111) FS [4]. In earlier calculations a cell that contains only the first neighbor Fe atoms to the P impurity, we found that the Fe-P chemical interaction is slightly stronger at the Fe(111) FS due to a shorter interatomic distance. However, as a result of the small size of the unit cell and the exclusion of impurity-induced structural relaxation, the calculated ΔE_b - ΔE_s was found to be negative (-1.1 eV/cell), in contrast with the known embrittling

potency of P in Fe.

In a subsequent calculation, we expanded the unit cell size for more realistic simulations (24 atoms/cell for the GB and 15 atoms/cell for the FS) [14]. By using the equilibrium geometry determined from DMol cluster calculations [8], we found that structural relaxation may reduce the total energy of the clean FeΣ3[1$\bar{1}$0] (111) (ie., the reference system for ΔE_b) by about 1.61 eV/cell. This, in turn, results in a large correction to ΔE_b. By contrast, the impurity atoms do not induce significant reconstruction for the less constrained environment of the Fe(111) surface [5] and thus ΔE_s is only slightly affected. As a result, $\Delta E_b - \Delta E_s$ becomes positive, 0.79 eV per P atom – in good agreement with experimental data.

In the present paper, we explore the mechanism of impurity-induced embrittlement more deeply by comparing the behaviors of P and B in the same FeΣ3[1$\bar{1}$0] (111) GB and Fe(111) FS environments. As B is known to be a GB cohesion enhancer in Fe [1–3], the comparison offers insights into the key electronic features underlying the influence of segregants on relative boundary cohesion. Following presentation of the model and computational details in Sec. II, we discuss the difference between B and P on the Fe boundary cohesion from the point of view of the calculated electronic and magnetic properties in Sec. III.

II. MODEL AND COMPUTATION

As sketched in Fig. 1, we used a slab model to simulate both the P/Fe(111) free surface and P/FeΣ3[1$\bar{1}$0] (111) GB, which minimizes GB interactions inherent in superlattice cells [4, 6]. For the B/Fe(111) and P/Fe(111) FS systems, the Fe(111) substrate is simulated by a 13 layer slab and the B and P adsorbates are placed pseudomorphically on the three-fold hollow sites on both sides of the slab. For the GB systems, a 23 layer slab is adopted to simulate the clean FeΣ3[1$\bar{1}$0] (111). With 12

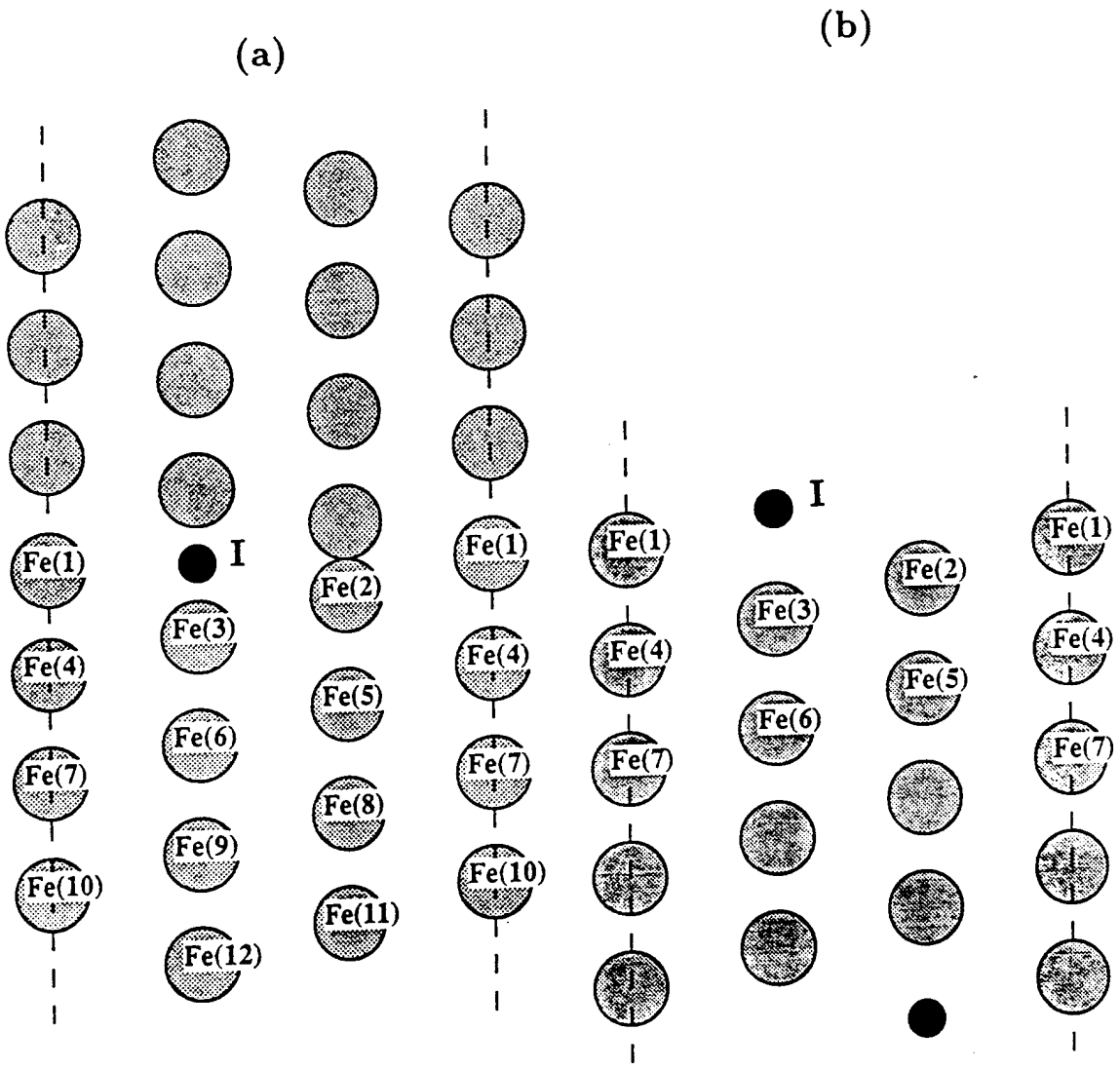

FIG. 1. Model and notation for the structure of Fe and impurities (I) at (a) Fe $\Sigma 3[1\bar{1}0]$ (111) "incoherent" twin boundary, and (b) Fe(111) free surface.

Fe layers in between, the interaction between the free surface (introduced artificially in the slab model) and the GB is expected to be sufficiently reduced. The 2D lattice constant and the unrelaxed Fe-Fe interatomic distance are chosen from experimental values for bulk bcc Fe, i.e., d_{Fe-Fe}=4.69 a.u. The slab models are sufficiently thick to allow multilayer atomic relaxation for Fe in both FS and GB environments. For the clean and impurity adsorbed Fe(111) surface, the equilibrium atomic geometry is determined through FLAPW total energy minimization [5, 7]. For grain boundary systems, geometries obtained from DMol cluster force calculations [8] are adopted.

In the FLAPW method [9], no shape approximations are made to the charge densities, potentials and matrix elements. The core states are treated fully relativistically and the valence states are treated semi-relativistically (i.e., without spin-orbit coupling) [10]. We employ the Hedin and Lundqvist and the von Barth−Hedin formulas for the exchange-correlation potentials for the nonmagnetic and the spin-polarized calculations, respectively [11]. This approach has been applied very successfully in the last decade to determine the electronic and magnetic properties of many transition metal systems. [12]

Energy cutoffs of 11 Ry and 70 Ry are employed for plane wave bases and star functions to describe the wave functions and the charge density and potential in the interstitial region, respectively. Within the muffin-tin (MT) spheres ($r_{MT,Fe}$ = 2.0 a.u., $r_{MT,P}$ = 1.8 a.u., $r_{MT,B}$ = 1.3 a.u.), lattice harmonics with angular-momentum l up to 8 are adopted. Convergence is assumed when the average root-mean-square difference between the input and output charge (spin) densities is less than 5×10^{-4} e/(a.u.)^3 (1×10^{-4} e/(a.u.)^3). The step-forward fixed-basis approach [13] is used to speed up the calculations.

III. CALCULATED RESULTS

A. Structural relaxation

In previous calculations [14, 8], we found that the clean FeΣ3[1$\bar{1}$0] (111) GB undergoes an ω phase transition which, in turn, results in an antiferromagnetic coupling in the core region of the GB. In addition, the P impurities strongly push the Fe atoms apart across the GB to form an "anti–ω" structure, corresponding to a metastable state of the clean FeΣ3[1$\bar{1}$0] (111) GB. As listed in Table 1, such a large reconstruction gives a large "mechanical energy" contribution to the final value of ΔE_b by 1.61 eV/cell. The mechanical energy contribution corresponds to the energy of the unrelaxed Fe boundary after impurity removed , relative to the relaxed clean Fe boundary.

Although the B impurity is significantly smaller than the P atom, it still cannot be well accommondated in the ω-Fe GB and some B-induced Fe reconstruction should also be expected. Indeed, the calculated B-Fe(3) bond length is 4.06 a.u., only 9% shorter than that between P-Fe(3), 4.42 a.u. [8]. Surprisingly, this smaller relaxation gives rise to an even larger mechanical energy in Table 1, 1.69 eV, compared to that in the P/Fe case for which the Fe structure becomes closer to the metastable anti-ω structure.

As found previously [4], the bond length is shorter in the FS environment than that in the GB: the calculated $d_{P-Fe(3)}$ in P/Fe(111) is 4.5 a.u. and $d_{B-Fe(3)}$ in B/Fe(111) is 3.44 a.u. However, since the impurity atoms have a large space for adjustment in the vacuum region, the mechanical effects are expected to be less important in the FS environment. Indeed, as also listed in Table 1, the mechanical energy for the surface, ΔE_s, is usually less than 0.2 eV/cell, even when the contributions from both the impurity relaxation and the impurity-induced Fe relaxation are considered [14].

TABLE I. Calculated binding energies (in eV) of P and B in the Fe GB and FS environment and the decompositions into chemical, mechanical and magnetic contributions

	ΔE_b	ΔE_s	$\Delta E_b - \Delta E_s$	Magnetic
P-Fe				
Unrelaxed (Chemical)				
NM	−8.16	−7.58	−0.58	−0.17
FM	−8.19	−7.44	−0.75	
Relaxation (Mechnical)				
NM	+2.19	+0.01	+2.18	−0.64
FM	+1.61	+0.07	+1.54	
Relaxed (Total)				
NM	−5.97	−7.57	+1.60	−0.81
FM	−6.58	−7.37	+0.79	
B-Fe				
Unrelaxed (Chemical)				
NM	−8.27	−6.46	−1.81	+0.30
FM	−8.18	−6.67	−1.51	
Relaxation (Mechnical)				
NM	+1.53	+0.10	+1.43	+0.08
FM	+1.69	+0.18	+1.51	
Relaxed (Total)				
NM	−6.74	−6.36	−0.38	+0.38
FM	−6.49	−6.49	+0.00	

B. Chemical interaction

The impurity induced charge redistributions for the P/Fe(111) and B/Fe(111) FS systems, obtained by subtracting the superimposed charge density from a free P or B monolayer and a clean Fe(111) surface from the self-consistent charge density for the corresponding adsorption system, are presented in Figs. 2(a) and 2(b), respectively. Contours with green, yellow, red and pink colors denote the positive charge density difference and those with light and dark blue colors represent the negative charge density difference. For P/Fe(111), strong charge accumulations are shown in the region between both P-Fe(3) and P-Fe(1) – indicating some chemical interaction between these atoms. The charge density at the inner region around the P atom is significantly decreased due to the effects of the surrounding Fe atoms. This apparent reverse-charge transfer contradicts a simple estimate from the electronegativity (2.19 for P and 1.83 for Fe). As demonstrated previously, these behaviors can be understood from the large spatial extension of the P-3p wave function, and thus the "embedding" character of the P-Fe bonding [14].

By contrast, since the B-2p wave function is more localized than the P-3p wave function, the B-Fe(3) bonding is more covalent-like. In addition, B has only one 2p electron while P possesses three 3p electrons. In the isolated monolayer geometry, the B-2p electron occupies the bonding $p_{x,y}$ states which leaves the non-bonding p_z state empty. However, the p_z state becomes lower in energy by hybridizing with the Fe(3)-d_{z^2} state and thus, as shown in Fig. 2(b) there is charge transfer from the in-plane $p_{x,y}$ states to the vertical p_z state. Therefore, B-Fe bonding in Fig. 2(b) shows much stronger spatial anisotropy compared to that between P-Fe in Fig. 2(a), i.e., stronger vertical B-Fe(3) bonding and weaker lateral B-Fe(1) bonding. As a result, the chemical part of E_s for B in the FS environment, 6.67 eV/adatom, is 0.77 eV smaller than that for P.

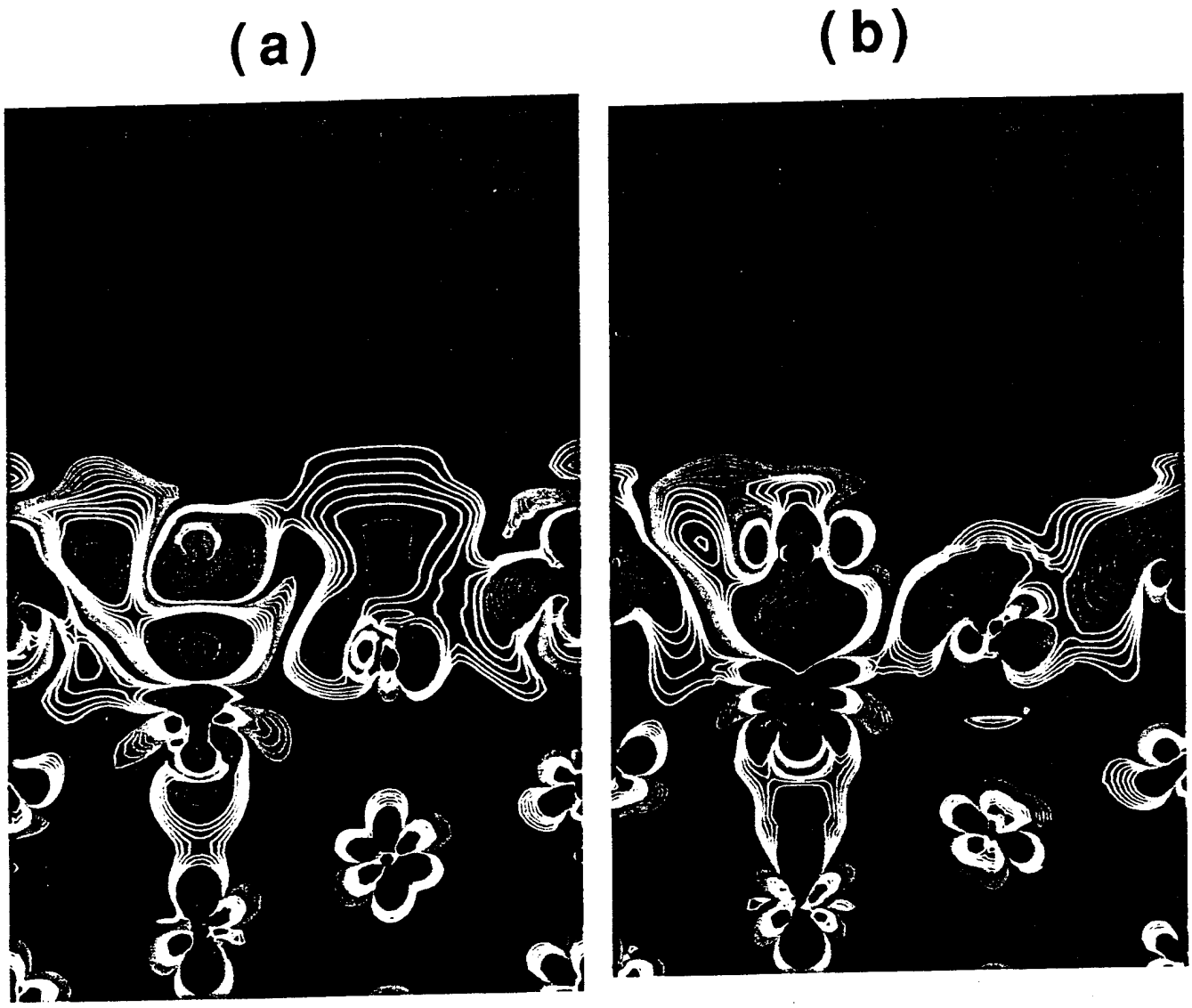

FIG. 2. The calculated valence charge density difference for the (a) P/Fe(111) and (b) B/Fe(111) FS systems. Contours start from 1×10^{-3} e/a.u.^{3} and increase successively by a factor of $2\frac{1}{4}$; green, yellow, red and pink colors denote positive differences and light and dark blue colors denote negative differences.

The corresponding charge density differences for P/Fe and B/Fe GB systems are presented in Figs. 3(a) and 3(b), respectively. Due to the longer bond length, the charge accumulation and hence the strength of Fe-impurity bonding are weaker compared to the case in the FS environment. However, there are two P(B)-Fe(3) bonds across the GB, which results in a larger chemical energy in the GB systems by 0.75 eV for P and 1.51 eV for B. Dramatically, although the B-Fe(1) interaction is much weaker compared to P-Fe(1) for the reason discussed above, the chemical energies for B and P in the GB environment become almost equal, 8.18 eV.

As found previously [4, 15], the presence of the impurity reduces the Fe(2)-Fe(2) interaction across the GB. In Fig. 2, the negative charge density difference can also be found above the Fe atoms in the FS environment. This charge removal was once proposed to explain the embrittlement effect of impurities on GB cohesion [15]. However, since this effect is even stronger for B which is a known GB cohesion enhancer in Fe, this does not appear to be an essential feature of embittlement behavior.

C. Magnetic interaction

In the previous small cell calculations [4], we found that P impurities strongly diminish the magnetization of their surrounding Fe atoms. This is still the case in the present large cell calculation. As shown in Fig. 4(a) by the spin density difference contours for the P/Fe GB, the detrimental effects of the P impurities on the magnetization around the Fe(1), Fe(2) and Fe(3) atoms are very clear. However, P induces an enhancement of magnetization around the second-rank Fe atoms, that was not obtained in the previous small cell calculations [4]. Note that this behavior is not seen in Fig. 3(a) for the charge density difference – indicating that the P induces a short-ranged perturbation (screening) for the charge distribution but shows a long-ranged oscillatory behavior for the magnetic disturbance. The spin density at

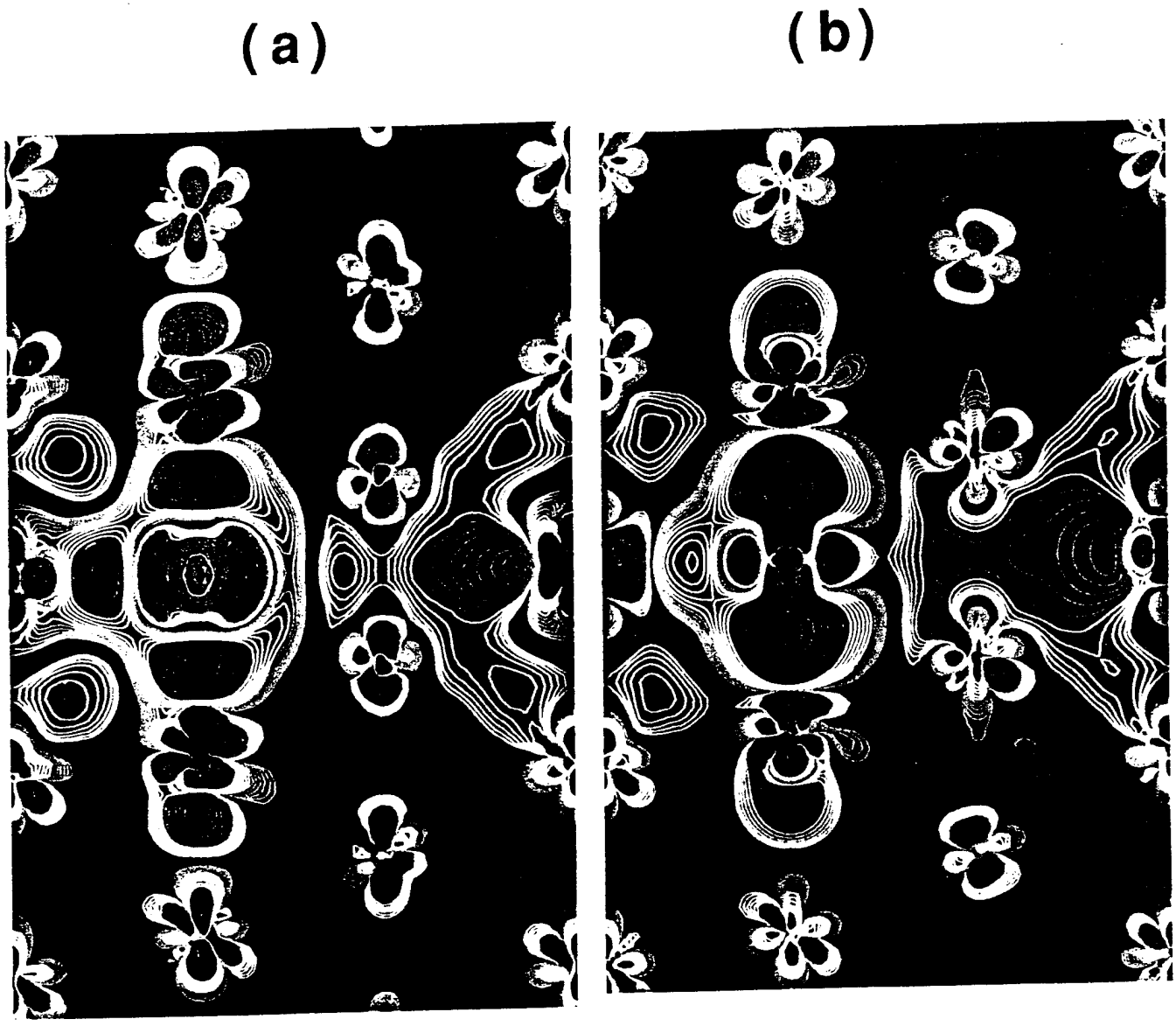

FIG. 3. The calculated valence charge density difference for (a) P/Fe and (b) B/Fe GB. Contours start from 1×10^{-3} e/a.u.^{3} and increase successively by a factor of $2^{\frac{1}{4}}$; green, yellow, red and pink colors denote positive differences and light and dark blue colors denote negative differences.

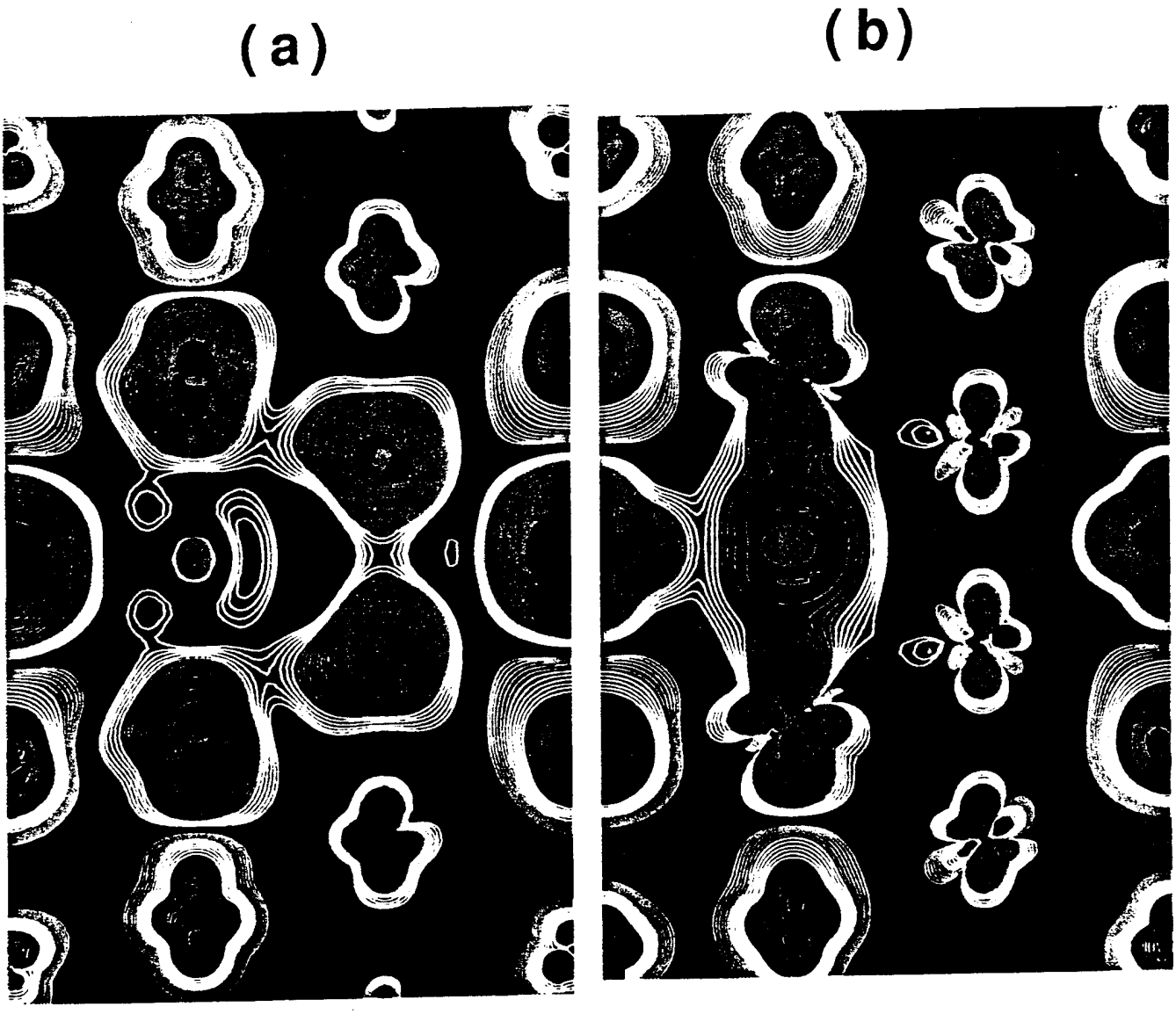

FIG. 4. The calculated spin density difference for (a) P/Fe and (b) B/Fe GB. Contours start from 1×10^{-3} e/a.u.^{3} and increase successively by a factor of $2^{\frac{1}{4}}$; green, yellow, red and pink colors denote positive differences and light and dark blue colors denote negative differences.

the P site is very small, so P does not carry a large magnetic moment (≈-0.01 μ_B) although its $3p$ band exhibits some exchange splitting [14]. By comparison, as shown in Fig. 3(b), B effects on the magnetization of the surrounding Fe atoms are weaker, especially for the Fe(2) atom. In addition, the magnitude of the negative spin density around the B site is not small. B carries a magnetic moment of -0.05 μ_B in its muffin-tin sphere. In Table 1, we can see from comparison of ferromagnetic (FM) and nonmagnetic (NM) calculations (i.e., with and without spin polarization) that the magnetic contributions to the segregation energies (magnetic energy) are very small, typically around 0.1 eV. However, this can be important in some case such as for the mechanical energy in the P case.

The spin density differences plotted in Figs. 5(a) and 5(b) for the P/Fe(111) and B/Fe(111) FS system show the same trend as that in Fig. 4, i.e., P and B adsorbates diminish (enhance) the magnetization around their first (second) rank Fe neighbors. However, the difference in magnitude is also obvious for both P and B. For P, the spin density around Fe(2) and Fe(1) is less affected in the FS environment, although the interatomic distances are smaller compared to those in the GB. By contrast, B affects Fe(2) and Fe(3) more strongly in the FS. As reflected in Table 1, the magnetic energy increment (with structural relaxation) for P/Fe(111) is 0.20 eV vs. -0.13 eV for B/Fe(111), while it is -0.61 eV for the P/Fe GB vs 0.25 eV for the B/Fe GB.

Quantitatively, the calculated magnetic moment in each Fe muffin-tin sphere is presented in Table 2. The effects of P are obvious since it reduces the magnetic moment of Fe(1) by 1.0 μ_B in both the GB and FS environments. In P/Fe(111), the P-induced decrease of the Fe(3) magnetic moment is also as large as 0.63 μ_B, which results in the positive magnetic contribution to ΔE_s. By comparison, the reduction of the Fe(3) magnetic moment is even a little larger in B/Fe(111), 0.65 μ_B. By contrast, B effects for the Fe(1) magnetic moment are reduced in the FS, 0.38 μ_B vs 0.45 μ_B

TABLE II. Calculated magnetic moments (in μ_B) in Fe. GB0 represents the relaxed clean Fe GB, while GB1 and GB2 denote the unrelaxed GB for P and B, respectively.

atom	Fe GB0	Fe GB1	P/Fe GB	Fe GB2	B/Fe GB	Fe(111)	P/Fe(111)	B/Fe(111)
Fe(1)	−1.28	2.40	1.40	2.50	2.05	2.71	1.74	2.33
Fe(2)	1.56	2.11	1.81	2.18	2.17	2.29	2.22	2.28
Fe(3)	1.43	1.81	1.49	2.07	1.90	2.36	1.73	1.71
Fe(4)	−1.75	1.81	2.01	1.86	2.15	2.20	2.30	2.31
Fe(5)	0.80	2.10	2.05	2.14	2.14	2.20	2.17	2.13
Fe(6)	1.42	1.85	1.98	1.85	2.02	2.11	2.27	2.29
Fe(7)	1.68	2.10	2.14	2.01	2.10	2.02	2.24	2.14

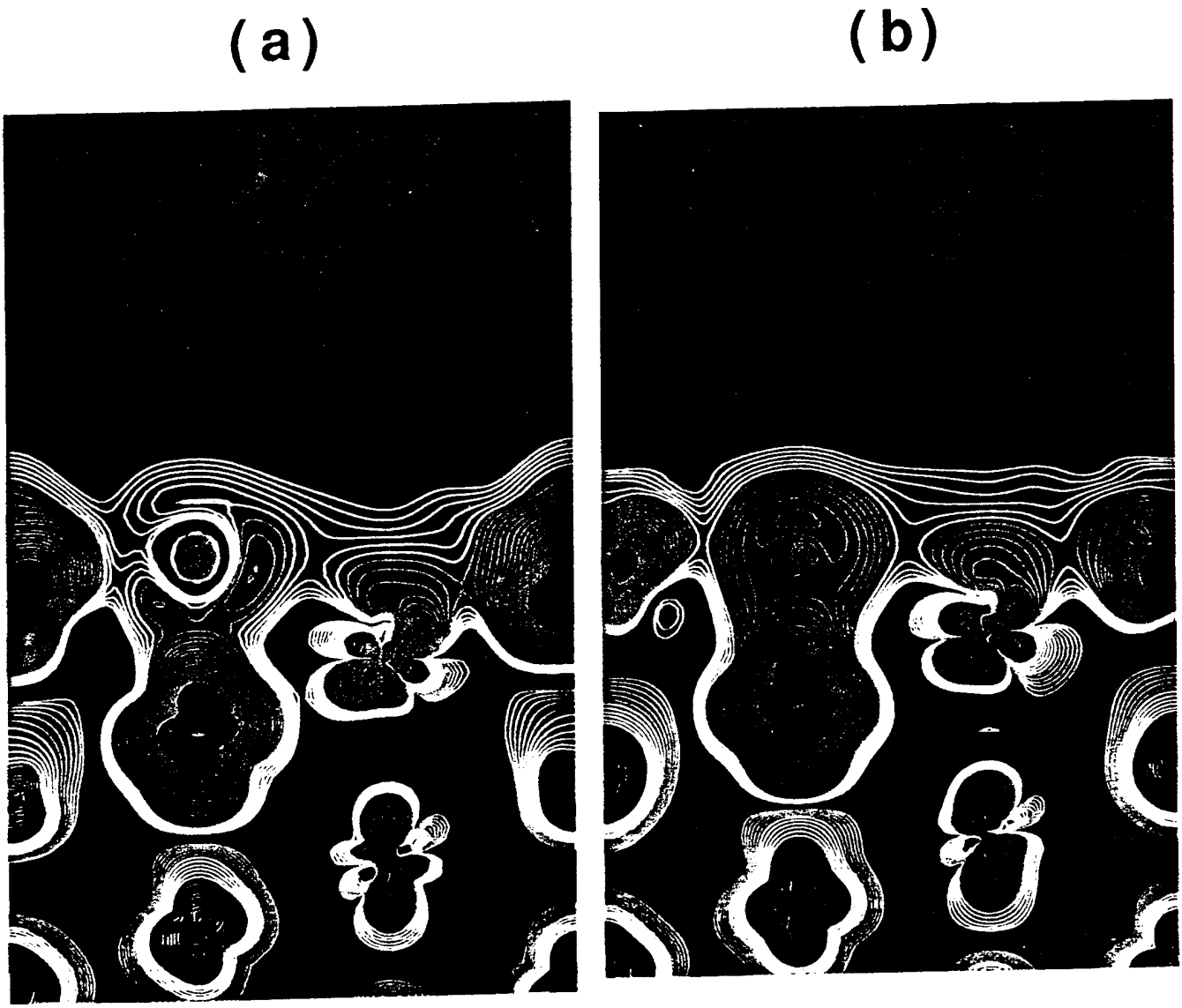

FIG. 5. The calculated spin density difference for (a) P/Fe(111) and (b) B/Fe(111) FS. Contours start from 1×10^{-3} e/a.u.^{3} and increase successively by a factor of $2^{\frac{1}{4}}$; green, yellow, red and pink colors denote positive differences and light and dark blue colors denote negative differences.

in the GB; this contributes a negative magnetic energy increment for ΔE_s of B since there are three Fe(1) atoms but only one Fe(3) atom at the surface. However, the magnetic moment enhances in both B/Fe GB and P/Fe GB if compared to the the strongly depressed value for the relaxed clean Fe GB due to the shorter interatomic distance and the antiferromagnetic coupling [14].

IV. SEGREGATION ENERGY AND DISCUSSION

Finally, the calculated results for the $\Delta E_b - \Delta E_s$ difference controlling embrittlement are listed in Table 1. Note that, by including the impurity-induced structural relaxation, the segregation energy for P in the grain boundary environment is smaller (less negative) than that on the free surface, i.e., $\Delta E_b - \Delta E_s = 0.79$ eV > 0, in good agreement with experiment (0.4±0.2 eV/cell). According to the Rice-Wang thermodynamic theory [1], P is thus an embrittler for the FeΣ3[1$\bar{1}$0] (111) GB. By contrast, $\Delta E_b - \Delta E_s$ is almost zero (negative for the nonmagnetic case) for B, and thus B is weakly cohesion enhancing. To our knowledge, this is the first quantitative theoretical explanation for the different behavior of B and P metalloid impurities on GB cohesion in Fe.

From the discussions above, many factors affect the final results of $\Delta E_b - \Delta E_s$. The mechanical energy is especially important, as the segregation energy differences are negative for both P and B when relaxation for the clean Fe GB is neglected. From Table 1, we can see that the magnetic energies are not large for either ΔE_b or ΔE_s separately, but are indeed important for their difference. Therefore, a highly-precise spin polarized method and, importantly, equal treatment for the FS and GB systems, are essential to obtain correct predictive results. The net magnetic contributions to the $\Delta E_b - \Delta E_s$ differences are summarized in the last column of Table 1. While magnetism reduces the embrittlement potency of P, it also reduces the cohesion enhancing

effect of B.

Impurity-induced reduction of Fe-Fe bonding is here eliminated as the mechanism for GB embrittlement. Since the embrittlement behavior of an impurity is determined by $\Delta E_b - \Delta E_s$, it is essential to compare the difference of effects in the FS and GB systems, respectively. In both the FeΣ3[1$\bar{1}$0] (111) GB and the Fe(111) FS, there are three Fe(1) atoms. The strength of impurity-Fe(1) bonding, seen from Figs. 2 and 3, does not change greatly from the GB to FS environments and thus is not significant for $\Delta E_g - \Delta E_s$. By contrast, impurity-Fe(3) bonding is expected to play the important role since one out of two of the vertical bonds is broken from the GB to FS. Therefore, the spatial anisotropy of the bonding interaction between the impurity states with the surrounding Fe atom can be crucial to embrittlement behavior. Simply, impurities with stronger vertical and weaker lateral bonding are favorable to enhance the GB cohesion.

This conclusion is supported by the comparison of P and B. In Fig. 3(b), the B-Fe(3) bonding is much stronger than the B-Fe(1) bonding. There is even a dangling bond above of the B atom for B/Fe(111) in Fig. 2(b). Therefore, B prefers the GB environment to saturate the B-Fe(3) bonding. By contrast, P-Fe bonding is more embedded-like (electrostatic) and thus there is no such dangling bond above P for P/Fe(111) in Fig. 2(a). In addition, the strength of the P-Fe(1) bonding is almost as strong as that of P-Fe(3) bonding. Only one out of five P-Fe bonds is broken from the GB to FS for P (one out of two for B) and thus the reduction of the chemical energy for P is smaller than for B. This is the main reason why the chemical part of $\Delta E_b - \Delta E_s$ for B is two times larger than that for P. Calculations for C and S impurities are in progress to verify the generality of these bonding trends.

V. ACKNOWLEDGEMENT

Work supported by the Office of Naval Research (Grant No. N00014-90-J-1363) with seed funding from the National Science Foundation MRL program (Grant No. DMR88-16126) and a grant of computer time (Cray-C90) at the NSF Pittsburgh Supercomputing Center from its Division of Advanced Scientific Computing.

REFERENCES

[1] J.R. Rice and J-S. Wang, Mat, Sci. & Eng., **A 107**, 23 (1989).

[2] P.M. Anderson, J-S. Wang and J.R. Rice, in *Innovations in Ultrahigh-strength Steel Technology*, ed. G.B. Olson, M. Azrin and E.S. Wright, Sagamore Army Materials Research Conference Proceedings: 34th (1990), p. 619.

[3] G.B. Olson, in *Innovations in Ultrahigh-strength Steel Technology*, ed. G.B. Olson, M. Azrin and E.S. Wright, Sagamore Army Materials Research Conference Proceedings: 34th (1990).

[4] R. Wu, A.J. Freeman and G.B. Olson, J. Mater. Res **7**, 2433 (1992).

[5] R. Wu, A.J. Freeman and G.B. Olson, Phys. Rev. B **47** 6855 (1993).

[6] G.L. Krasko and G.B. Olson, Solid State Comm. **76**, 247 (1990).

[7] R. Wu and A.J. Freeman, Phys. Rev. B **47** 3904 (1993).

[8] S.P. Tang, A.J. Freeman and G.B. Olson, Phys. Rev. B **47**, 2441 (1993).

[9] E. Wimmer, H. Krakauer, M. Weinert and A.J. Freeman, Phys. Rev. B **24**, 864 (1981), and references therein.

[10] D.D. Koelling and B.N. Harmon, J. Phys. C **10**, 3107 (1977).

[11] U. von Barth and L. Hedin, J. Phys. C **5**, 1629 (1972).

[12] A.J. Freeman and R. Wu, J. Magn. Magn. Mater. **100**, 497 (1992).

[13] R. Wu and A.J. Freeman, Comput. Phys. Commun **76** 58 (1993).

[14] R. Wu, A.J. Freeman and G.B. Olson, Phys. Rev. B, submitted.

[15] C.L. Briant and R.P. Messmer, Phil. Mag. B **42**, 569 (1980).

APPENDIX B

Submitted to Phys. Rev. B

542.tex; January 3, 1994

Local Density Studies of the Structure and Electronic Properties of B and S in an Fe Grain Boundary

Shaoping Tang and A.J. Freeman

Department of Physics and Astronomy

Northwestern University

Evanston, Illinois 60208-3112

and

G.B. Olson

Department of Materials Science and Engineering

Northwestern University

Evanston, Illinois 60208

Abstract

The structure and electronic properties of B and S impurities in an Fe $\Sigma 3[1\bar{1}0](111)$ grain boundary are studied using the DMol molecular cluster method. A large cluster containing 91 atoms is used to simulate the local environment of the boundary. Optimized atomic geometries are obtained by atomic force calculations. The results show that impurities induce large relaxations in the grain boundary, and that the electronic structure of the hybridized B/Fe system is very different from that of the non-hybridized S/Fe system.

PACS Numbers: 61.70.-r, 61.70.Ng, 71.55.-i

I. Introduction

It is well known that impurities such as P, S, Sn and Sb cause intergranular embrittlement of Fe, while C and B enhance the intergranular cohesion in iron and alloy steels.[1] Because of its importance to grain-boundary sensitive properties such as the stress-corrosion resistance of ultrahigh-strength steels, the mechanism underlying these phenomena has been the subject of considerable research effort.[2–10,14] It has become evident from these studies that the desired understanding will require detailed consideration of precise grain boundary atomic structure and energetics coupled with underlying electronic level structure and properties.

Recent theoretical efforts have applied first principles electronic structure calculations to study the role of impurities in the embrittlement of Fe and proved to be very useful in elucidating possible mechanisms of Fe embrittlement.[6–10] One of the major obstacles in using the first principles approach, however, has been the need for substantial computing power not available until recently. With the rapid development of computer technology, one can now perform such calculations with reasonable cost.

In a previous paper, we applied the first principles DMol molecular cluster method to study phosphorus induced structural changes in the Fe grain boundary (GB).[10] It was shown that P induces large relaxations in the GB, and the electronic structure of the GB also changes significantly. In this paper, we compare the effects of B and S impurities on the Fe $\Sigma 3[1\bar{1}0](111)$ grain boundary using the same theoretical techniques: We first determine the atomic relaxation induced by the impurities using atomic force calculations; the electronic structure is then calculated for the relaxed structure. Previous electronic structure calculations used relatively small clusters[3–7] and did not consider the role of lattice relaxation.[8,9] Those studies provided useful information on the bonding between the metal and impurities. However, as the large relaxations induced by impurities may

also change the electronic structure of the Fe GB, consideration of atomic relaxation is necessary for a correct description of the electronic structure.

II. Methodology

We use the DMol method[11] which is a first-principles numerical method for solving the local density functional equations and is capable of calculating analytic energy gradients[12] for each atom within the cluster model. The Hedin-Lundqvist exchange correlation potential[13] is employed with the frozen-core approximation. We use extended basis sets for the B, S and Fe atoms, ie., a double set of valence functions plus a single d polarization function for B and S atoms and a single p function for Fe. The binding energy of a cluster is defined as $E_b = -(E_t - E_a)$ where E_t is the total energy of the cluster and E_a is the sum of atomic total energies. For a given atomic geometry, the binding energy of the system and the forces on atoms of interest are calculated. To find the optimized geometry, the atoms are further displaced according to the forces acting on them. An optimized structure is obtained when all the forces acting on the atoms are sufficiently small. In this work, the degree of self-consistent convergence is measured by root mean square (rms) changes in the charge density; it is set to 10^{-5} which allows the total energy to converge to 10^{-5} Ry. The force convergence criterion is 6.0×10^{-3} Ry/a.u..

The grain boundary considered is the $\Sigma 3[1\bar{1}0](111)$ "incoherent" twin boundary as treated in previous studies.[8–10,14] The 91 atom cluster model contains 17 layers of Fe adjacent to the grain boundary and is shown in Fig.1. The impurity atoms are placed at the center of the trigonal prism formed by iron atoms in the GB core, and D_{3h} symmetry is used. In searching for the optimum geometry, the boundary atoms of the cluster are fixed in their bulk positions. When we refer to the relaxation of a particular atom, say, Fe_{11}, other atoms satisfying D_{3h} group operations have

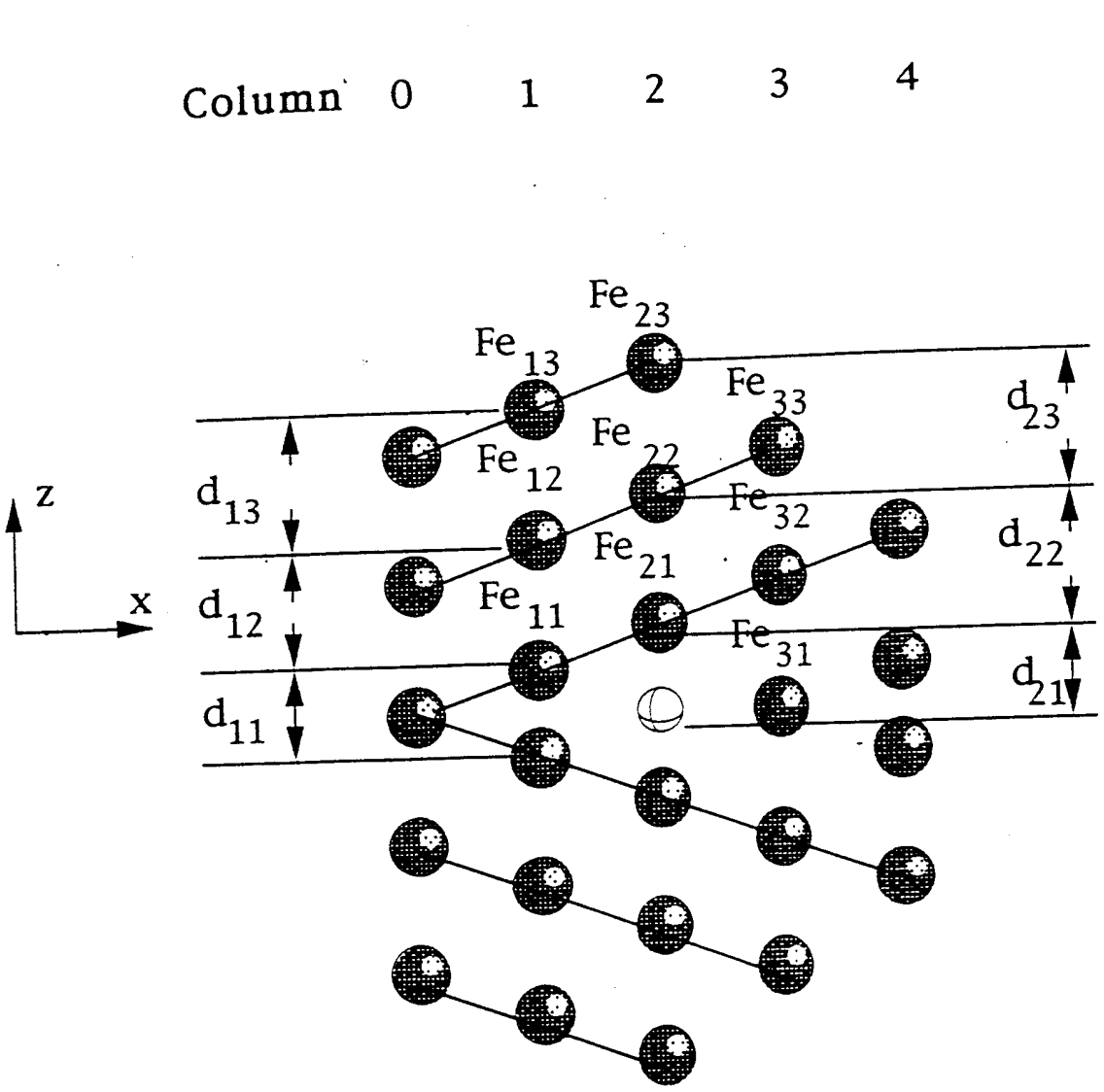

FIG. 1. Side view of the 91 atom cluster simulating the Fe grain boundary. The impurity atom is put in the center of the trigonal prism formed by Fe atoms in the GB core. Atoms in each Fe layer are not shown in the figure.

the same relaxation as Fe_{11}.

III. Results and Discussion

A. Atomic relaxation study

The relaxation study is carried out by force calculations in which atoms in columns 1 and 2 in Fig. 1 can relax along the z direction since those atoms are most affected by the impurity in the GB center. For the B/Fe system, we first calculate the relaxation of Fe atoms using a 53 atom cluster which takes less computing time. Since the interlayer distance and the bond length between impurity and Fe atoms are underestimated using the 53 atoms cluster as previously shown in the P/Fe system,[10] the result from the small cluster is used as an initial input for the 91 atoms cluster calculation. The final optimized structural information is presented in Table I. For the S/Fe system, we use the P/Fe system data for the 91 atom cluster[10] as initial input, anticipating that S and P induce similar relaxations.

The basic relaxation results are: 1) for the clean GB structure, there are two structures having energy minima. One corresponds to the case in which two center Fe atoms (Fe_{21}) move towards the GB center, referred to as GB-1. This gives a structure for the $\Sigma 3$ GB core which is very similar to the ω phase observed in Ti alloys. The other structure corresponds to Fe_{21} atoms moving apart from the GB center (an "anti-ω" structure), referred to as GB-2. It has been shown that the GB-1 structure is more stable energetically than the GB-2 structure.[10] Here, we also allow the Fe_{32} atoms to relax along the z direction in the GB-1 structure. It is found that the calculated results show an average difference of less than 1% for structural data and very small changes for binding energy compared to the GB-1 structure displayed in Table I. Hence, the extra relaxation of the Fe_{32} atoms causes only slight changes for the clean GB structure. 2) When impurities are introduced in the

center of the GB, the Fe atoms directly above the impurity (Fe_{21} atoms) are pushed outwards from the center (favoring the GB-2 structure), and this affects the atoms in the outer layer. The net effect is that almost all Fe atoms are relaxed outwards from the center. 3) S induces larger relaxation for atoms near the impurity (eg., d_{11} and d_{21}) than does B as shown in Table I. The Fe atom (Fe_{21}) directly above the impurity relaxes outwards 42% for S/Fe and 30% for B/Fe compared with its initial (unrelaxed coincidence site lattice) position. The bond length between Fe_{21} and B is 2.15Å and is smaller than that between Fe_{21} and S (2.35Å).

The relaxation results can be compared with an empirical calculation using a modified Embedded Atom Method (EAM) by Krasko.[14] The EAM calculations show that for the clean GB, the stable structure corresponds to the down position of Fe_{21} which agrees with our GB-1 structure. After B and S are put in the center of the GB, the EAM also found that S induces larger relaxation of Fe atoms near the impurity than does B. The calculated bond length between Fe_{21} and B and between Fe_{21} and S from the EAM are 1.96Å and 2.60Å respectively, which has an average difference of 10% with the results of the present calculation. Our bond length value for Fe_{21} and S (2.35Å) may increase if an even larger cluster is used. As can be seen from Table I, the distance between the boundary atoms and the nearest inner atoms in the z direction are compressed (ie. d_{13} and d_{23}) compared to the bulk value of 2.48Å. It is quite possible that the boundary atoms will be pushed further outwards when a larger cluster is used. If that is true, we can expect a weakening of the vertical interaction between Fe_{21} and S. This may be useful in elucidating the mechanism of S embrittlement since the competition between bonding in the vertical and horizontal directions is an important factor.

It is worth mentioning that although B is a light element, it has a higher binding energy (1.71 eV) in the Fe GB than does S. This is due to the shorter Fe_{21} and B bond length that results in the stronger interaction between B and Fe. Similar results were obtained for the binding energy

of B and S in Ni by Painter and Averill[6] which showed that B binds in the Ni host much more strongly (7.0 eV) than does S (2.2 eV) and produces a smaller expansion of the host cluster than does S.

B. Charge density and density of states

Figure 2 shows the charge density difference plotted in the $(1\bar{1}0)$ plane containing the impurity and several neighboring Fe atoms. (The charge density difference is calculated by subtracting from the charge density of the impurity in the GB, the pure GB charge density and a single impurity charge density placed at the center of the GB so that the impurity-induced charge redistribution can be seen more clearly.) Comparing the charge density difference between the B/Fe and S/Fe systems, we can see that there is one common feature for the two systems: the interaction of impurity and Fe atoms is restricted to a local region near the impurity, although the lattice relaxation is known to extend beyond this area.[14]

The main difference between them is the charge distribution in the vertical (z) and horizontal (x) directions. In Fig.2(a), B is seen to form relatively strong covalent-like bonding states with Fe atoms in the vertical direction and a much weaker bonding with Fe atoms in the horizontal direction. In the S/Fe system (see Fig.2(b)), slightly more charge is accumulated in the region between S and Fe_{31} atoms than between S and Fe_{21} atoms, giving the impression that the bonding along the horizontal direction is stronger than that along the vertical direction, although the distance between S and the Fe atoms in both directions are almost equal. The same phenomenon was found for the P/Fe system calculated both from the full-potential linearized augmented plane wave (FLAPW[9]) and DMol[10] method. It is doubtful that these charge accumulations represent strong covalent bonding between S and Fe since the density of states (DOS) curves presented below do

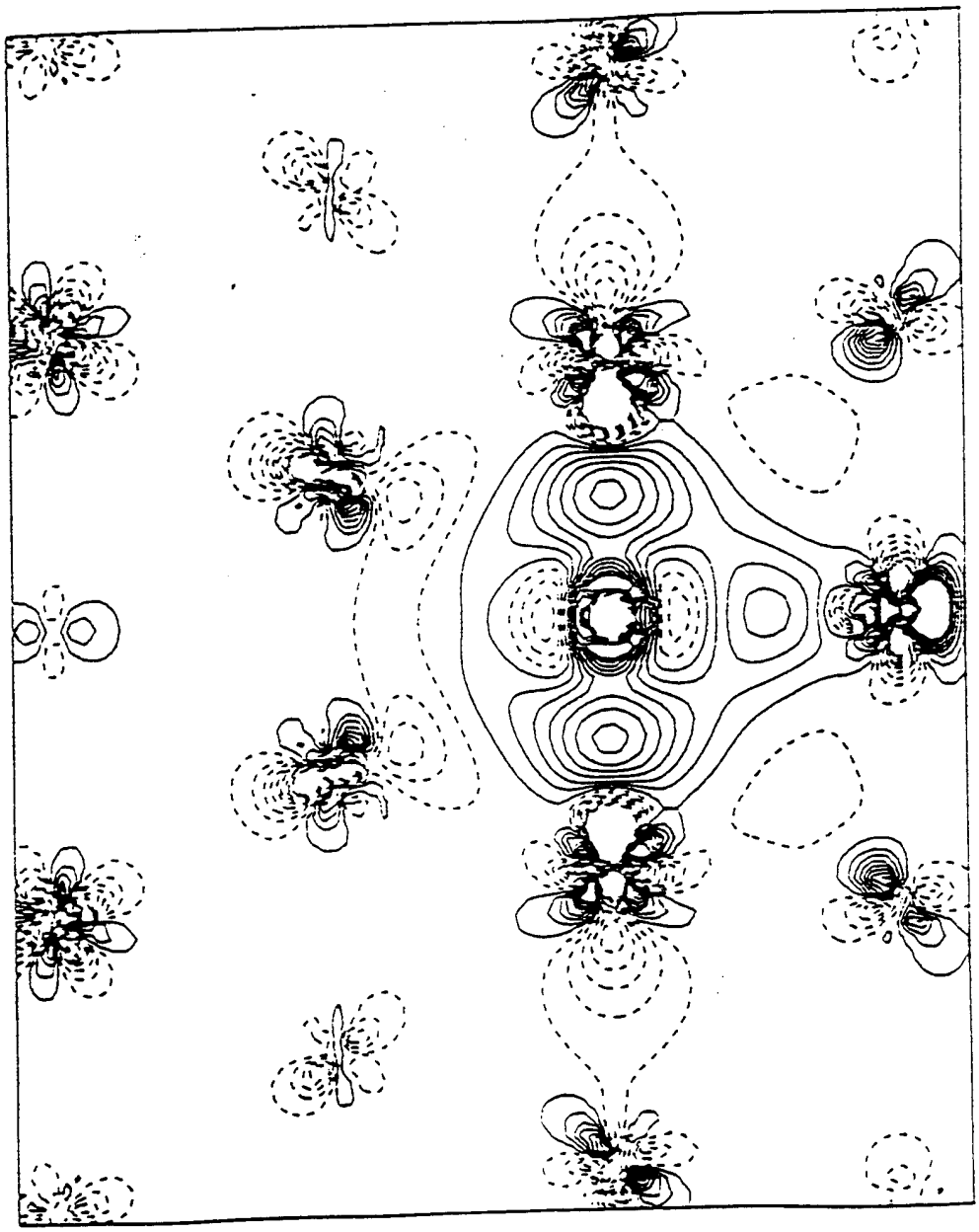

FIG. 2. Charge density difference between impurity in the GB and a superposition of a single impurity and pure GB calculated from the 91 atom cluster. The plots are in a plane containing the impurity, Fe_{11}, Fe_{21} and Fe_{31} atoms. The contour spacings are $0.002e/(a.u.)^3$. Solid lines mean again of charge, and dashed lines mean a loss of charge. (a) B/Fe.

not confirm the hybridization between S and Fe.

To understand this, we plot the two molecular orbitals containing mainly S-3p electron contributions in Fig.3(a) and Fig.3(b). In Fig.3(a), one can see a dominant S-3p_z-like wave function having only weak bonding with Fe_{31}; a similar dominant S-3p_x-like wave function is seen in Fig.3(b). Hence, the bonding between S and Fe is weak. If we compare Fig.3 with the free atom S-3p wave function (not shown here), we find that the free S-3p wave function has greater spatial expansion. When S is in the Fe GB environment, the S-3p electrons will feel the repulsive interaction of nearby Fe electrons and shrink towards the S nucleus, and so there is some charge accumulation in the region between the Fe and S atoms.

Note that the charge accumulation in the region between S and Fe is acompanied by a decrease of charge in the S center region as can be seen from Fig.2(b). To estimate how the charges are distributed, we calculate the Mulliken electron population; the results show that there is about 0.37e charge redistribution from S-3s and S-3p states to the high energy S-3d state. This will reduce the charge in the center region compared to the free S atom which results in the image of Fig.2(b).

Figures 4 and 5 show the calculated partial density of states (DOS) for B, S and several nearby Fe atoms. The DOS of the clean GB (i.e., GB-1) is shown by dashed lines and the DOS of single B and S are also shown by dashed lines in Figs. 4a and 5a, respectively. For S in the Fe GB, the main S-3s peak (not shown) lies well below the d states of Fe, and thus has no hybridization with Fe. The majority of the S-3p states and a small portion of S-3s states are at the tail end of the Fe states, again showing a weak interaction with Fe. For B in the Fe GB, the B-2s electron has very little overlap with Fe, while B-2p forms broadly hybridized states with Fe d states between -2 to -5.5 eV. This is in agreement with the charge density picture shown in Fig.2(a). To obtain

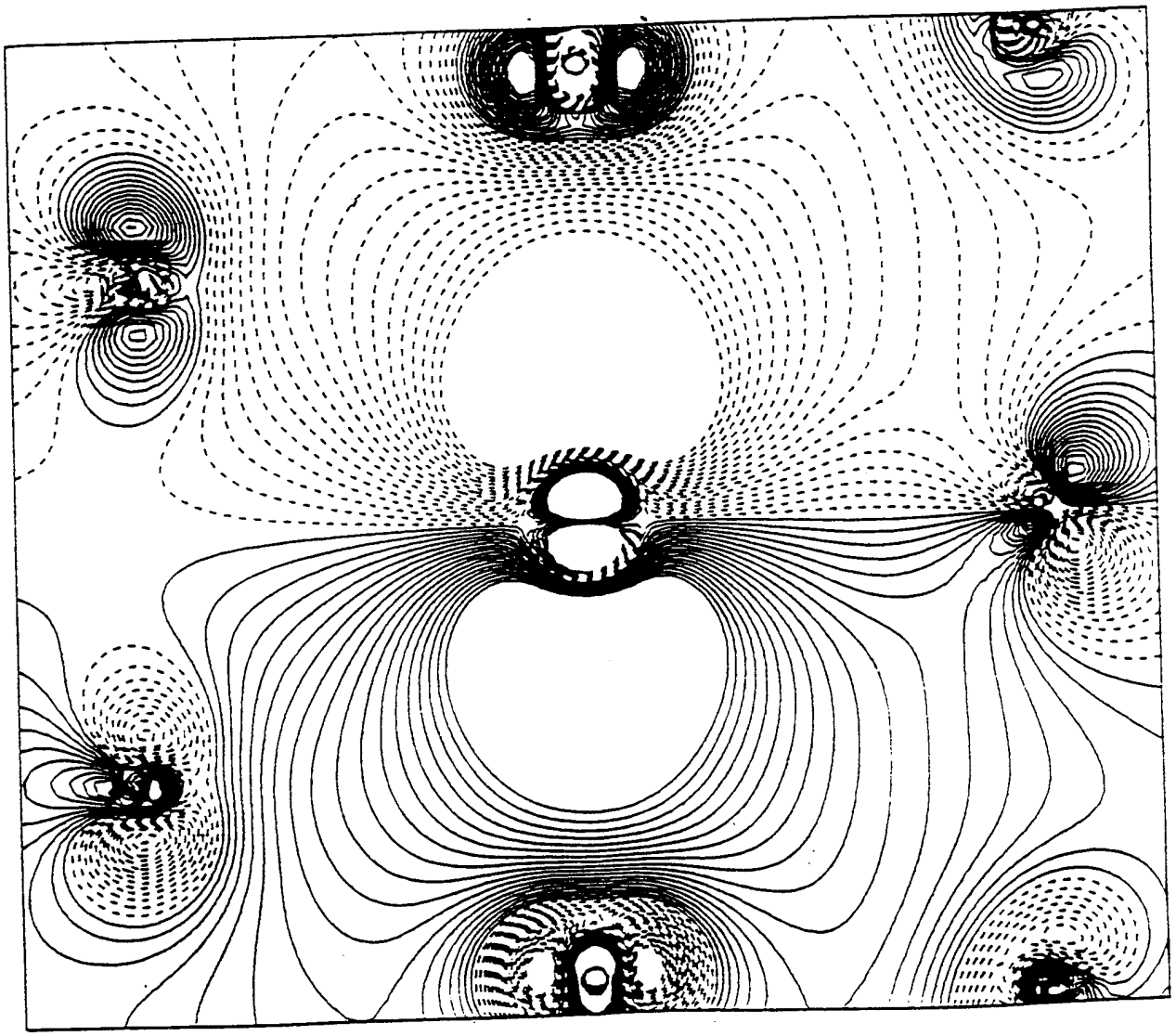

FIG. 3. Contour plot of molecular orbitals for S in the Fe GB. The contour spacing is 0.004. (a) $1a_2''$ orbital.

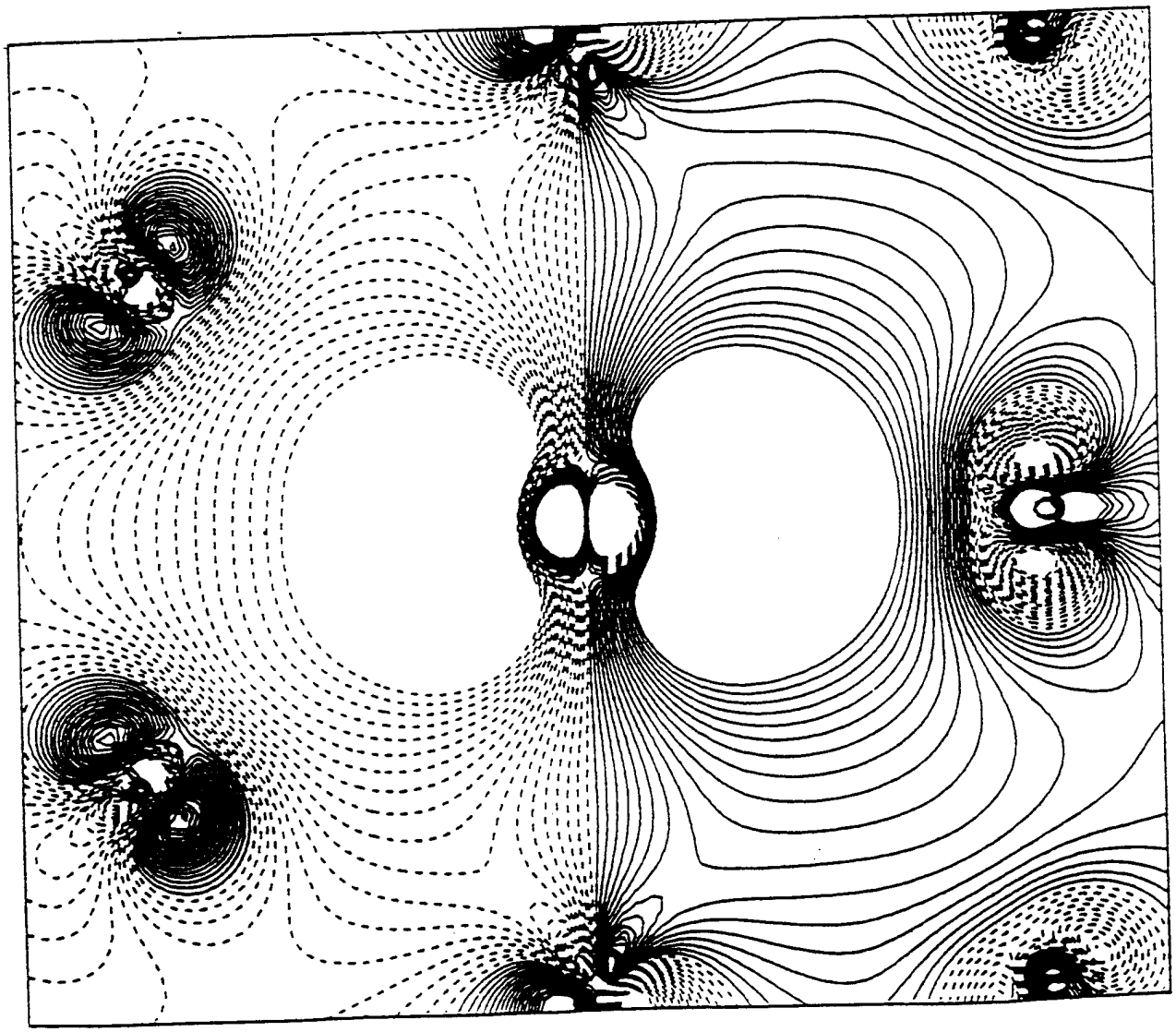

FIG. 3. Contour plot of molecular orbitals for S in the Fe GB. The contour spacing is 0.004. (b) $1e'$ orbital.

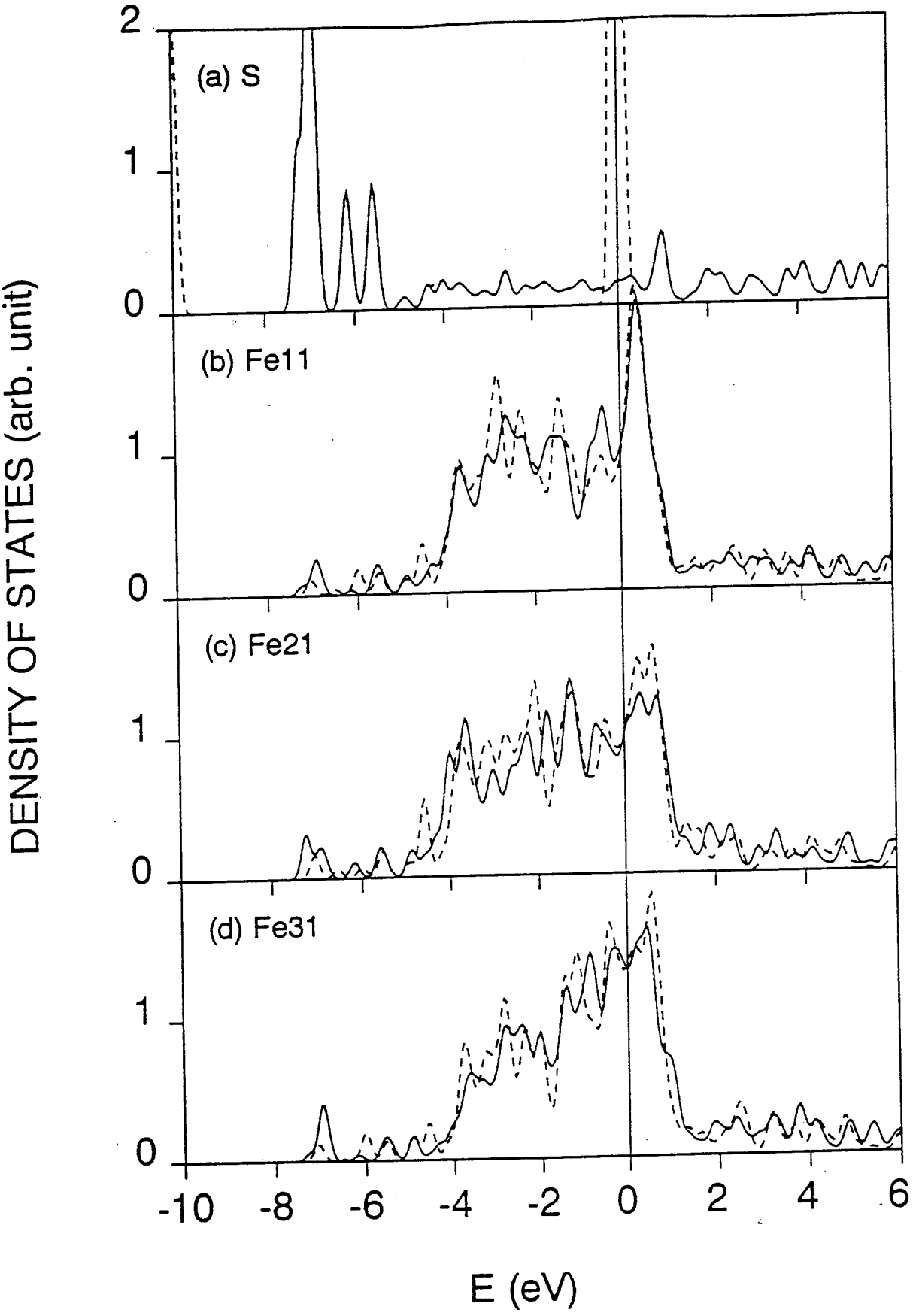

FIG. 4. The partial density of states for S in the Fe GB.

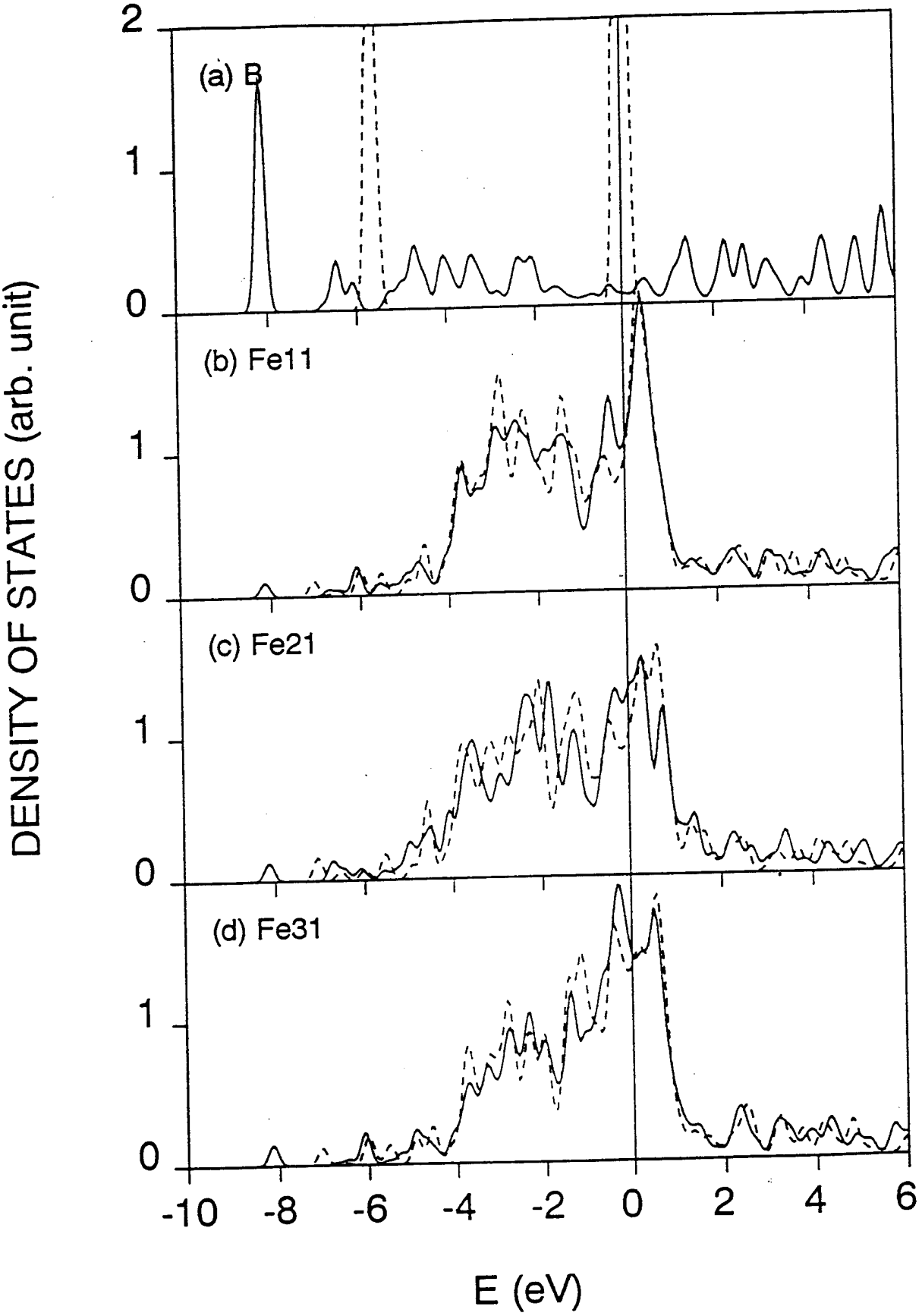

FIG. 5. The partial density of states for B in the Fe GB.

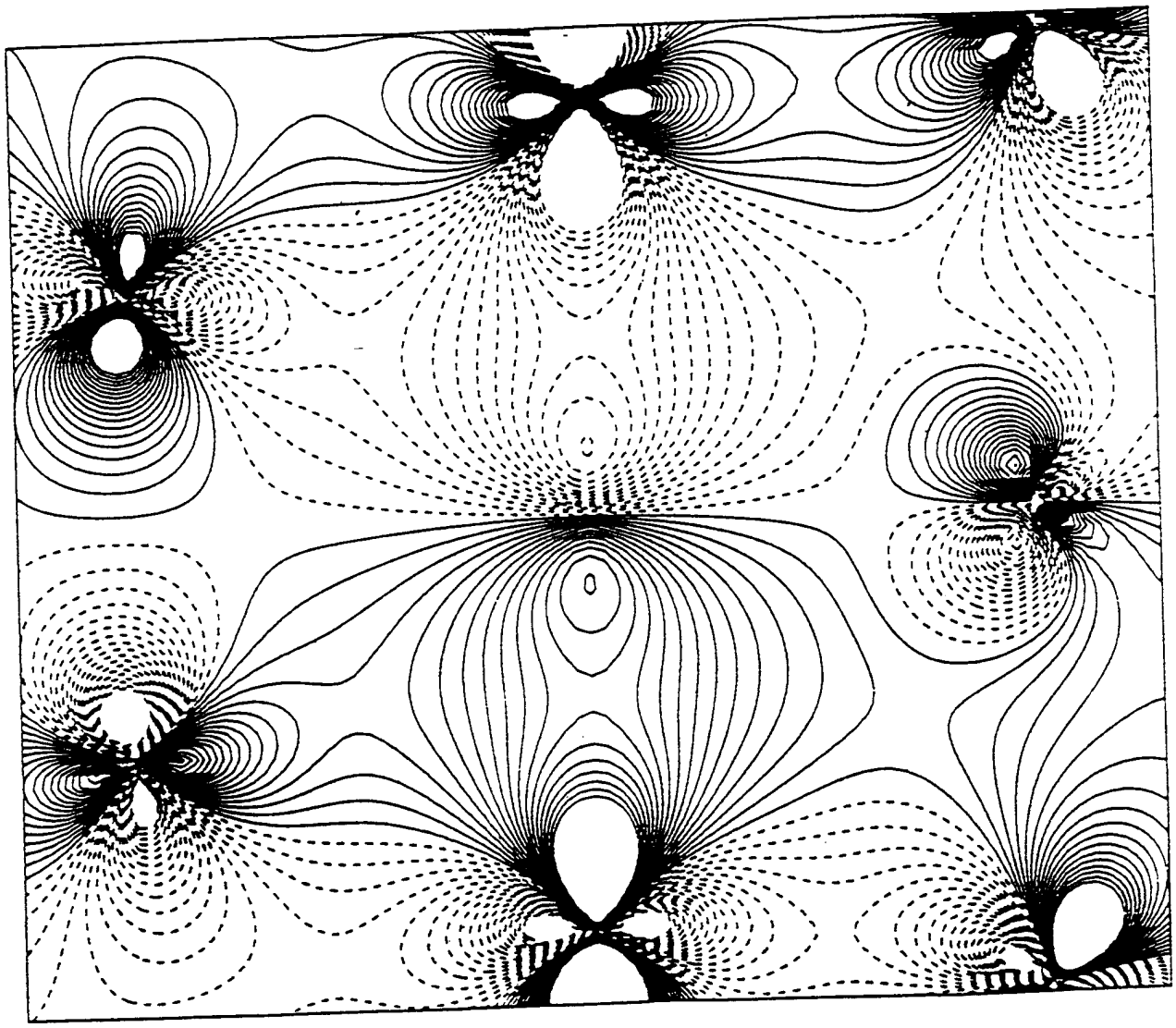

FIG. 6. Contour plot of the $10a_2''$ molecular orbital for B in the Fe GB. The contour spacing is 0.004.

insight into how B bonds with Fe, we plot in Fig. 6 the $10a_2''$ orbital which is located 2.82 eV below E_F. It is clearly seen that B-$2p_z$ and Fe-$3d_{z^2}$ form a σ bonding state in the vertical direction in contrast with Fig.3(a) which shows that the S-$3p_z$ states dominate the area between S and Fe without overlapping with the Fe states.

In summary, we have performed first principles local density DMol molecular cluster calculations on the role of the B and S impurities in the Fe grain boundary. When impurities are placed in the center of the GB, it is found that B induces less relaxation for nearby Fe atoms than does S. The nearest distance between B and Fe and between S and Fe are 2.15Å and 2.35Å, respectively. For the bonding between impurities and Fe, we found that B-$2p_z$ forms a relatively strong σ bonding with Fe_{21}-$3p_{z^2}$, while S has very little hybridization with Fe, resulting in a weak bonding state. These differences in electronic structure for B and S may be useful in understanding their different effects on grain boundary cohesion.

Acknowledgments

This work was supported by the Office of Naval Research (Grant No. N00014-90-J-1363), and by a computing grant at the Pittsburgh Supercomputing Center, supported by the NSF Division for Advanced Scientific Computing.

References

[1]G.B. Olson, in Innovations in Ultrahigh-strength Steel Technology, ed. G.B. Olson, M. Azrin and E.S. Wright, Sagamore Army Material Research Conference Proceedings: 34th(1990), and references therein.

[2]J.R. Rice and J-S. Wang, Mat. Sci.& Eng., **A 107**, 23(1989).

[3]R.P. Messmer, Phy.Rev. B **23**, 1616(1981).

[4]R.P. Messmer and C.L. Briant, Acta Metall. **30**, 457(1982).

[5]A. Collins, R.C. O'Handley and K.H. Johnson, Phys. Rev. B **38**, 3665(1988).

[6]G.S. Painter and F.W. Averill, Phy. Rev. Lett. **58**, 234(1987).

[7]M.E. Eberhart and D.D. Vvedensky, Phys. Rev. lett. **58**, 61(1987).

[8]G.L. Krasko and G.B. Olson, Solid State Comm. **76**, 247(1990).

[9]R. Wu, A.J. Freeman and G.B. Olson, J. Mater. Res.**7**, 2403 (1992).

[10]S. Tang, A.J. Freeman and G.B. Olson, Phys. Rev. B **47**, 2441(1993).

[11]B. Delley, J. Chem. Phys. **92**, 508 (1990).

[12]B. Delley J. Chem. Phys. **94**,7245(1991).

[13]L. Hedin and B.I. Lundqvist, J. Phys. C**4**, 2064 (1971).

[14]G.L. Krasko, in *Structure and Properties of Interfaces in Materials*, edited by W.A.T. Clark, U. Dahmen and C.L. Briant, MRS Symposia Proceedings No. 238 (Materials Research Society, Pittsburgh, 1991), p. 481

Tables

TABLE I. Calculated structural parameters (in Å) for the 91 atom cluster model defined in Fig.1. The "initial" distances are calculated from the unrelaxed coincidence site lattice structure. GB-1 refers to the geometry when Fe_{21} relaxes inward towards the center of the GB and GB-B and GB-S refer to the cases when B and S are added to the GB; d_{Fe} is the distance between the two near-center atoms in column 2 in the pure GB and E_b is the binding energy in eV.

	initial	GB-1	GB-B	GB-S
d_{11}	1.65	2.49	2.48	2.61
d_{12}	2.48	2.47	2.41	2.35
d_{13}	2.48	2.07	2.14	2.14
d_{21}	—	—	2.15	2.35
d_{22}	2.48	2.48	2.46	2.30
d_{23}	2.48	2.93	2.01	1.97
d_{Fe}	3.31	2.43	—	—
E_b	—	421.86	428.67	426.96